Properties of c-C_4F_8 inductively coupled plasmas. II. Plasma chemistry and reaction mechanism for modeling of Ar/c-C_4F_8/O_2 discharges

Alex V. Vasenkov[a)]
University of Illinois, Department of Electrical and Computer Engineering, 1406 West Green Street, Urbana, Illinois 61801

Xi Li and Gottlieb S. Oehrlein
Department of Materials Science and Engineering and Institute for Research in Electronics and Applied Physics, University of Maryland, College Park, Maryland 20742-2115

Mark J. Kushner[b)]
University of Illinois, Department of Electrical and Computer Engineering, 1406 West Green Street, Urbana, Illinois 61801

(Received 12 September 2003; accepted 9 February 2004; published 27 April 2004)

Gas mixtures containing Ar, c-C_4F_8, O_2, and CO are often used for the plasma etching of silicon dioxide. Gas phase reaction mechanisms are required for first principles modeling of these systems to both provide insights to the plasma chemistry and to help optimize the process. In this article, results from computational and experimental investigations of the plasma chemistry of inductively coupled plasmas (ICPs) sustained in Ar, O_2, Ar/c-C_4F_8 and O_2/c-C_4F_8 gas mixtures with and without magnetic confinement are discussed. These results were used to develop a reaction mechanism for low-pressure and low-temperature plasmas sustained in mixtures initially consisting of any combination of Ar/c-C_4F_8/O_2/CO. Predictions for ion saturation current and ion mass fractions were compared to experiments for validation. The consequences of charge exchange of fluorocarbon species with Ar^+ and CO^+ on the ratio of light to heavy fluorocarbon ion densities in Ar/c-C_4F_8/O_2/CO plasmas are discussed. We found that the electron density and ion saturation current significantly increase with the addition of Ar to c-C_4F_8 but weakly depend on the addition of O_2. The ratio of light to heavy fluorocarbon ion densities increases with power, especially for ICPs with magnetic confinement. [DOI: 10.1116/1.1697483]

I. INTRODUCTION

Low-pressure fluorocarbon plasmas are widely used in microelectronics fabrication for a variety of surface modification purposes.[1–4] In particular, fluorocarbon plasmas are used for the etching of dielectric materials. The choice of the initial fluorocarbon gas in these plasmas is usually based on obtaining optimum ratios of fluxes of polymerizing radicals, material removing radicals and activating energetic ions. These parameters also determine the selectivity of etching one material compared to another. For example, selective etching of SiO_2 compared to Si in fluorocarbon plasmas usually results from the deposition of thicker polymer layers on Si relative to SiO_2. The SiO_2 etch process consumes the CF_x overlayer, thereby thinning the polymer, and allowing more efficient penetration of activating ion fluxes to the SiO_2-polymer interface. Si being less reactive with the polymer, is overlaid with a thicker polymer which transmits fewer reactants and less activation energy.[5,6]

Subtle variations of these processes for different materials (e.g., etching of SiO_2 vs Si_3N_4) have resulted in the use of a wide variety of fluorocarbon gases (e.g., CHF_3, C_2F_6, and c-C_4F_8) and numerous additives (e.g., O_2, N_2, CO, and Ar) to optimize the reactant fluxes and delivery of activation energy.[4,7,8] The use of some of these additives is the result of empirical parametrization. For example, addition of Ar can be used to regulate the ratios of polymerizing radical flux to ion flux. The use of O_2 regulates the thickness of the polymer by O atom etching of deposited layers.[4]

Cyclic-C_4F_8 (c-C_4F_8) is commonly used in microelectronics fabrication for plasma etching of dielectrics such as silicon dioxide and silicon nitride.[4,6] The c-C_4F_8 is readily dissociated by electron impact, forming polymerizing radicals that increase etch selectivity. These c-C_4F_8 plasmas are also used for cleaning reactors after SiO_2 deposition. In this regard c-C_4F_8 is often used in mixtures with Ar, CO, N_2, and O_2. Modeling of c-C_4F_8 containing plasmas is of interest for the design of reactors and processes, and to provide insight into the complex chemistry occurring in these mixtures. It is also a challenging task as only limited data are available for electron-CF_x and CF_x-CF_x radical collisions.[9–16] Previous computational studies of c-C_4F_8 inductively coupled plasmas (ICPs) have been reported by Kazumi, Hamasaki, and Tago,[17] Font, Morgan, and Mennenga,[14] and Rauf and Ventzek.[16]

Kazumi and co-workers developed a reaction mechanism for the modeling of c-C_4F_8 plasmas in which the dissociation pathways and threshold energies were determined using molecular orbital theory.[17] The mechanism was used to predict the densities of CF_x radicals in microwave discharges sustained in c-C_4F_8, Ar/c-C_4F_8, and He/c-C_4F_8. Reactions of fluorocarbon neutral and ion species with Ar and He ad-

a)Present address: CFD Research Corp., 215 Wynn Drive, Huntsville, AL 35805; electronic mail: avv@cfdrc.com
b)Author to whom correspondence should be addressed; electronic mail: mjk@uiuc.edu

ditives were neglected in an attempt to simplify the mechanism. A strong correlation between the concentrations of fluorocarbon radicals and etch selectivity were observed.

A set of cross sections for electron collisions with c-C_4F_8 based on a combination of calculations, beam measurements, and swarm analysis, and a reaction mechanism for fluorocarbon species were developed by Font and co-workers.[14] The mechanism was employed in a two-dimensional model for inductively coupled plasmas (ICPs). The authors validated their mechanism against experiments performed in the Gaseous Electronic Conference (GEC) reference cell. The model reproduced the major experimental trends observed by Hebner[18] by predicting that CF_2^+ and $C_2F_4^+$ are the dominant positive ions and that F^- is the dominant negative ion.

Rauf and Ventzek performed a computational investigation of ICP discharges sustained in Ar/c-C_4F_8.[16] Good agreement was obtained with experiments performed in the GEC reference cell, and CF_2 was identified as the dominant CF_x radical in c-C_4F_8 discharges. The Ar/c-C_4F_8 plasmas were found to be mildly electronegative, becoming more electropositive with an increase of Ar.

In this article we discuss results from a computational and experimental investigation of the plasma chemistry in ICPs sustained in c-C_4F_8, Ar/c-C_4F_8, O_2/c-C_4F_8, and Ar/c-C_4F_8/O_2/CO mixtures. The strategy we followed was to validate the model using measurements first made in ICPs separately sustained in Ar and O_2, for which electron impact and heavy particle reactions are well known, and then in plasmas with more complex chemistry such as c-C_4F_8, Ar/c-C_4F_8 and O_2/c-C_4F_8. We found that ion saturation currents are significantly larger in Ar plasmas than in O_2 and c-C_4F_8 plasmas for the same conditions. Consequently, the ion currents increase with the addition of Ar to c-C_4F_8, but weakly depend on the addition of O_2 to c-C_4F_8. Computational results also demonstrated that the ratio of light ion to heavy ion densities increases with power, especially for ICPs with permanent magnets, in agreement with experiments. The mechanism is sensitive to the branching ratios for dissociation of both feedstock gases and their fragments, and to charge exchange of Ar^+ with fluorocarbon radicals. A brief description of the model is given in Sec. II and the reaction mechanism is discussed in Sec. III. A description of the experimental techniques and more extensive experimental results are in a companion paper, Part I.[19] The results of this investigation are discussed in Sec. IV. Concluding remarks are in Sec. V.

II. DESCRIPTION OF THE MODEL

The two-dimensional Hybrid Plasma Equipment Model (HPEM) used in this study was previously described in detail in Ref. 20 and references therein, and so only an outline will be given here. The HPEM consists of the Electromagnetic Module (EMM), the Electron Energy Transport Module (EETM), and Fluid–chemical Kinetics Module (FKM). The EMM solves Maxwell equations for radio frequency (rf) magnetic and electric fields using a frequency domain approach. Static magnetic fields are also computed in the EMM. When using static magnetic fields, the conductivities in Maxwell equations are tensors depending on these fields. The rf fields are transferred to the EETM where electron transport coefficients and source functions are obtained from electron energy distributions produced either by an electron Monte Carlo simulation or by solving the electron energy equation with transport coefficients obtained from a two-term spherical harmonic expansion of Boltzmann equation. In this study, the energy equation was used in the vast majority of cases since the modeling of complex chemistry sustained, for example, in Ar/c-C_4F_8/O_2/CO mixtures, is a large computational burden. The electron transport coefficients are transferred from the EETM to the FKM, which solves the continuity, momentum, and energy equations for neutral and charged species, and Poisson's equation for the electric potential. Flow was directly calculated by having flux sources at the gas inlet and flux sinks at the pump ports. The boundary conditions for pumping were specified assuming constant pressure and mass flow through the reactor. The modules are iterated until a converged solution is obtained.

The computed ion densities and temperatures in the HPEM were used to determine the net ion saturation current for comparison to experimental probe measurements. This current is defined as being proportional to the flux of ions crossing the surface area A_p of a cylindrical probe[21]

$$I=\frac{1}{4}\,\delta\sqrt{\frac{2\pi T_e}{eT_i}}A_p\sum_j\ n_j q_j v_j\,, \tag{1}$$

where e is the base of natural logarithm, index j is for the summation over all positive ions. The terms q_j, n_j and v_j are the charge, density and thermal velocity of the jth ion. T_i and T_e are the averaged ion and electron temperatures. The parameter δ depends on the probe collecting voltage V_p and probe radius[21]

$$\delta=\frac{r_s+r_p}{r_p}\left[\operatorname{erf}\left(\frac{-\eta}{(r_s+r_p)^2/r_p^2-1}\right)^{1/2}+\frac{r_p}{r_s}\exp(-\eta)\operatorname{erf}\left(\frac{-\eta(r_s+r_p)^2}{(r_s+r_p)^2-r_p^2}\right)^{1/2}\right], \tag{2}$$

where r_p is the probe radius and $\eta=qV_p/kT_i$. The sheath thickness r_s was estimated using the Child Law model[22]

$$r_s=\frac{\sqrt{2}}{3}\lambda_D\left(\frac{2V_p}{kT_e}\right)^{3/4}. \tag{3}$$

The Debye length λ_D depends on electron temperature T_e and electron density n_e:

$$\lambda_D=743\sqrt{\frac{T_e}{n_e}}\,(\mathrm{cm}), \tag{4}$$

where T_e is in eV and n_e is in cm^{-3}. The ion saturation current determined by Eq. (1) is larger than the Langmuir current by the factor $\sqrt{2\pi T_e/eT_i}$ due to the effective area of the pre-sheath, where ions are accelerated to the Bohm speed by the large ambipolar fields.[21]

TABLE I. Species in the plasma chemistry mechanism.

Argon species	Oxygen species	COF_x species
Ar	O_2	CO
Ar*(4s)	O_2^+	CO^+
Ar**(4p)	O_2^-	CO_2
Ar^+	$O_2^*(^1\Delta)$	COF
	O	COF_2
	$O^*(^1D)$	FO
	O^+	
	O^-	
Carbon species	F_x species	CF_x species
C	F	CF
C^+	F^+	CF^+
	F^-	CF_2
	F_2	CF_2^+
	F_2^+	CF_3
		CF_3^-
		CF_3^+
		CF_4
C_xF_y species		
$C_2F_3^+$	$C_3F_5^+$	$C_4F_7^+$
C_2F_4	C_3F_6	C_4F_8
$C_2F_4^+$	$C_3F_6^+$	$C_4F_8^-$
C_2F_5	C_3F_7	$C_4F_8^-$*
$C_2F_5^+$	$C_3F_7^+$	$C_4F_8^+$
C_2F_6	C_4F_7	
C_3F_5		

III. REACTION MECHANISM

A reaction mechanism was developed for plasmas sustained in gas mixtures initially consisting of arbitrary mole fractions of Ar/c-C_4F_8/O_2/CO. The limited electron impact cross-section data for the fluorocarbon species were collected and synthesized. Rate coefficients for gas phase chemistry were taken from independent studies in the literature or estimated from measurements for related species. Although this mechanism is intended for low-pressure plasma applications (<10s mTorr) it is likely valid to pressures exceeding many Torr. In general, our approach was to include only the major species which influence plasma properties and reactant fluxes in order to minimize computational time. Since the computational time is less sensitive to the number of reactions, our mechanism is more exhaustive in that regard. Special care was taken to avoid so-called terminal species which are produced but not consumed in the mechanism.

The species used in the model are given in Table I. All pertinent electron impact events which affect electron transport, such as elastic collisions, vibrational and electron excitations, are included in the EETM. Only those excited states which were judged to be significant to the plasma chemistry reaction mechanism were explicitly tracked in the FKM. For example, mass spectrometric studies have recently identified the presence of large fluorocarbon ions and neutrals in fluorocarbon plasmas,[23–27] and it was reported that these large fluorocarbon ions partially control film growth during plasma etching of silicon.[28] We therefore included large ions whose abundances were observed in these experiments in order to investigate their effects on surface reactions. On the other hand, the formation of precursors to dust particles, such as C_xF_y with $x>4$, $y>8$, was neglected as their formation is less likely in the pressure range of interest (≤10s mTorr).

A. Electron impact reactions

Electron impact reactions for collisions with Ar, CO, O_2, C, F_x, CF_x and C_xF_y and their fragments are listed in Table II.[14,29–49] A schematic of the c-C_4F_8 electron impact reaction mechanism is shown in Fig. 1. The thickness of arrows represents the rates of electron impact reactions calculated for an ICP sustained in c-C_4F_8 at 6 mTorr, 600 W, and 13.56 MHz, and are indicative of the large variety of ions formed as a result of electron impact reactions. The electron impact cross sections for c-C_4F_8, reviewed in Ref. 12 are shown in Fig. 2, and were assembled using a combination of calculations,[14,50] mass spectrometry measurements,[47] and swarm analysis.[14]

Electron beam measurements have shown evidence for the formation of $C_4F_8^-$ by electrons with energies below 1 eV.[51] This ion is formed as a result of collisional relaxation of $C_4F_8^-$* which is initially formed by electron capture. The lifetime of $C_4F_8^-$* for autodetachment was measured as short as 10 μs using time-of-flight mass spectrometry and longer than 200 μs using an ion-cyclotron resonance method.[51,52] We estimated the rate of this process as $2\times10^6\,s^{-1}$. Time-of-flight mass spectrometry and laser photodetachment measurements indicate that the major negative ion formed by dissociative attachment of c-C_4F_8 is F^-. The concentrations of other branching to negative ions such as CF_3^-, $C_2F_3^-$, $C_3F_5^-$ were observed to be lower and these branchings are not included in the model.[51,53,54] This is, however, an approximation which could be improved upon in subsequent work. The c-C_4F_8 branching to F^- is important for the conditions of interest since its cross section peaks at about 7 eV which is close to the mean energy of electrons in low-pressure c-C_4F_8 plasmas.

Vibrational excitation is the most important c-C_4F_8 inelastic process below about 10 eV. Based on cross sections derived from swarm data this cross section was analytically represented by[55]

$$\sigma_j(E)=a_0\frac{f_0}{w_jE}[1-(w_j/E)^\alpha]^\beta\Phi(E,w), \tag{5}$$

where $a_0=6.513\times10^{-14}\,eV^2\,cm^2$ and w_j is the excitation threshold. Φ for vibrational excitation is

$$\Phi(E,w)=(E/w_j)^{I-\Omega}. \tag{6}$$

The values of f_0, α, β, Ω were determined by fitting the cross section data to Eqs. (5) and (6) and they are listed in Table II.

Using mass spectrometry Toyoda, Iio, and Sugai[56] and Jiao, Garscadden, and Haaland[47] detected $C_2F_4^+$, $C_3F_5^+$, CF_3^+, CF^+, CF_2^+ as the major products of dissociative ionization of c-C_4F_8. The parent ion c-$C_4F_8^+$ was not observed indicating that the ground state of c-$C_4F_8^+$ is likely not bound in the Franck–Condon region. The cross sections obtained by Toyoda and co-workers[56] and Jiao and

TABLE II. Electron impact excitation, ionization, and dissociation.[a]

Reaction	Rate coefficient[b]	Reference
Collisions with argon		
$e+Ar \rightarrow Ar+e$	c	49
$e+Ar \rightarrow Ar^*+e$	c	29
$e+Ar \rightarrow Ar^{**}+e$	c	29
$e+Ar \rightarrow Ar^+ +e+e$	c	30
$e+Ar^* \rightarrow Ar^+ +e+e$	c	31
$e+Ar^* \rightarrow Ar+e$	c	29[d]
$e+Ar^* \rightarrow Ar^{**}+e$	c	32
$e+Ar^{**} \rightarrow Ar+e$	c	29[d]
$e+Ar^{**} \rightarrow Ar^+ +e+e$	c	33
$e+Ar^{**} \rightarrow Ar^*+e$	c	32[d]
Collisions with oxygen		
$e+O_2 \rightarrow O_2+e$	c	34
$e+O_2 \rightarrow O_2(v)+e$	c	34
$e+O_2 \rightarrow O^- +O$	c	34
$e+O_2 \rightarrow O_2^* +e$	c	34
$e+O_2 \rightarrow O+O+e$	c	34
$e+O_2 \rightarrow O^*+O+e$	c	34
$e+O_2 \rightarrow O_2^+ +e+e$	c	34
$e+O_2 \rightarrow O^+ +O+e+e$	c	35
$e+O_2+M \rightarrow O_2^- +M$	$3.6\times10^{-31}\,T_e^{-0.5}\ \mathrm{cm^6\ s^{-1}}$	62
$e+O_2^* \rightarrow O_2+e$	c	34[d]
$e+O_2^* \rightarrow O_2^+ +e+e$	$1.3\times10^{-9}\,T_e^{1.1}\exp(-11.1/T_e)$	33,63
$e+O \rightarrow O^*+e$	c	64
$e+O \rightarrow O^+ +e+e$	c	64
$e+O^* \rightarrow O+e$	c	64[d]
$e+O^* \rightarrow O^+ +e+e$	c	64
$e+O^- \rightarrow O+e+e$	$1.95\times10^{-12}\,T_e^{-0.5}\exp(-3.4/T_e)$	63
Collisions with carbon and carbon monoxide		
$e+C \rightarrow C^+ +e+e$	$6.74\times10^{-9}\,T_e^{0.7}\exp(-11.26/T_e)$	36
$e+CO \rightarrow CO+e$	c	37,48
$e+CO \rightarrow C+O+e$	c	37
$e+CO \rightarrow CO^+ +e+e$	c	37
$e+CO \rightarrow C+O^+ +e+e$	c	37
$e+CO \rightarrow C^+ +O+e+e$	c	37
Collisions with F_x		
$e+F \rightarrow F+e$	c	38
$e+F \rightarrow F(ex)+e$	c	38
$e+F \rightarrow F^+ +e+e$	c	38
$e+F_2 \rightarrow F_2+e$	c	39
$e+F_2 \rightarrow F_2(v)+e$	c	39
$e+F_2 \rightarrow F_2(ex)+e$	c	39
$e+F_2 \rightarrow F_2+e$	c	39
$e+F_2 \rightarrow F^- +F$	c	39
$e+F_2 \rightarrow F_2^+ +e+e$	c	39
Collisions with CF_x		
$e+CF \rightarrow CF+e$	c	65[e]
$e+CF \rightarrow CF(v)+e$	c	65[e]
$e+CF \rightarrow C+F+e$	c	65[e]
$e+CF \rightarrow CF^+ +e+e$	c	40
$e+CF_2 \rightarrow CF_2+e$	c	42[f]
$e+CF_2 \rightarrow CF_2(v)+e$	c	42[f]
$e+CF_2 \rightarrow CF+F^-$	c	42[f]
$e+CF_2 \rightarrow CF+F+e$	c	42[f]
$e+CF_2 \rightarrow CF_2^+ +e+e$	c	41
$e+CF_2 \rightarrow CF^+ +F+e+e$	c	41
$e+CF_3 \rightarrow CF_3+e$	c	42[f]
$e+CF_3 \rightarrow CF_3(v)+e$	c	42[f]
$e+CF_3 \rightarrow CF_2+F+e$	c	42[f]
$e+CF_3 \rightarrow CF_3^+ +e+e$	c	41
$e+CF_3 \rightarrow CF_2^+ +F+e+e$	c	41
$e+CF_3 \rightarrow CF_2+F^-$	c	42[f]
$e+CF_4 \rightarrow CF_4+e$	c	42
$e+CF_4 \rightarrow CF_4(v)+e$	c	42
$e+CF_4 \rightarrow CF_3+F^-$	c	42
$e+CF_4 \rightarrow CF_3^- +F$	c	42

TABLE II. (*Continued*).

Reaction	Rate coefficient[b]	Reference
$e+CF_4 \rightarrow CF_3+F+e$	c	42
$e+CF_4 \rightarrow CF_3^+ +F+e+e$	c	42
$e+CF_4 \rightarrow CF_2+F+F+e$	c	42
$e+CF_4 \rightarrow CF_3^+ +F^- +e$	c	42
$e+CF_4 \rightarrow CF+F+F_2+e$	c	42
Collisions with C_xF_y		
$e+C_2F_3 \rightarrow CF+CF_2+e$	$1\times10^{-8}\,T_e^{0.91}\exp(-5.0/T_e)$	43[g]
$e+C_2F_4 \rightarrow C_2F_4+e$	c	15, 59
$e+C_2F_4 \rightarrow C_2F_4(v)+e$	c	15, 59
$e+C_2F_4 \rightarrow CF_2+CF_2+e$	c	15, 59
$e+C_2F_4 \rightarrow C_2F_4^+ +e+e$	c	15, 59
$e+C_2F_4 \rightarrow C_2F_3^+ +F+e$	c	15, 59
$e+C_2F_4 \rightarrow CF^+ +CF_3+e+e$	c	15, 59
$e+C_2F_5 \rightarrow C_2F_5+e$	c	45[h]
$e+C_2F_5 \rightarrow C_2F_5(v)+e$	c	45[h]
$e+C_2F_5 \rightarrow CF_3^- +CF_2$	c	45[h]
$e+C_2F_5 \rightarrow CF_3+CF_2+e$	c	45[h]
$e+C_2F_5 \rightarrow CF_3^+ +CF_2+e+e$	c	44
$e+C_2F_5 \rightarrow C_2F_5^+ +e+e$	c	44
$e+C_2F_6 \rightarrow CF_3^+ +CF_3+e+e$	c	45
$e+C_2F_6 \rightarrow C_2F_6+e$	c	45
$e+C_2F_6 \rightarrow C_2F_6(v)+e$	c	45
$e+C_2F_6 \rightarrow CF_3+CF_3^-$	c	45
$e+C_2F_6 \rightarrow C_2F_5+F^-$	c	45
$e+C_2F_6 \rightarrow CF_3+CF_3+e$	c	45
$e+C_3F_5 \rightarrow C_2F_3+CF_2+e$	$1.8\times10^{-8}\,T_e^{0.52}\exp(-12.3/T_e)$	15, 59[g,i]
$e+C_3F_5 \rightarrow C_2F_4+CF+e$	$1.8\times10^{-8}\,T_e^{0.52}\exp(-12.3/T_e)$	15, 59[g,i]
$e+C_3F_6 \rightarrow C_2F_6^+ +e+e$	$1.4\times10^{-8}\,T_e^{0.68}\exp(-10.6/T_e)$	15, 59[g,i]
$e+C_3F_6 \rightarrow C_2F_3+CF_3+e$	$1.8\times10^{-8}\,T_e^{0.52}\exp(-12.3/T_e)$	15, 59[g,i]
$e+C_3F_6 \rightarrow C_2F_4+CF_2+e$	$1.8\times10^{-8}\,T_e^{0.52}\exp(-12.3/T_e)$	15, 59[g,i]
$e+C_3F_7 \rightarrow C_2F_4+CF_3+e$	$1.8\times10^{-8}\,T_e^{0.52}\exp(-12.3/T_e)$	15, 59[g,i]
$e+C_4F_7 \rightarrow C_2F_4+C_2F_3+e$	$5.7\times10^{-8}\,T_e^{0.28}\exp(-8.0/T_e)$	45[g,h]
$e+C_4F_7 \rightarrow C_4F_7^+ +e+e$	$1.4\times10^{-8}\,T_e^{0.68}\exp(-10.6/T_e)$	45[g,h]
$e+C_4F_8 \rightarrow C_4F_8+e$	c	14
$e+C_4F_8 \rightarrow C_4F_8(v)+e$	c	14
$e+C_4F_8 \rightarrow C_2F_4+C_2F_4+e$	c	14[j]
$e+C_4F_8 \rightarrow C_4F_8^{-*}$	c	14
$e+C_4F_8 \rightarrow F^- +C_4F_7$	c	14
$e+C_4F_8 \rightarrow C_3F_5^+ +CF_3+e+e$	c	47
$e+C_4F_8 \rightarrow C_2F_4^+ +C_2F_4+e+e$	c	47
$e+C_4F_8 \rightarrow F^+ +C_4F_7+e+e$	c	47
$e+C_4F_8 \rightarrow CF_3^+ +C_3F_5+e+e$	c	47
$e+C_4F_8 \rightarrow CF_2^+ +C_3F_6+e+e$	c	47
$e+C_4F_8 \rightarrow CF^+ +C_3F_7+e+e$	c	47

Fitting parameters used in Eqs. (1)–(3)

	$C_4F_8(v)$	C_4F_8 (dissociation)	$C_2F_4(v1)$	$C_2F_4(v2)$
f_0	0.0339	0.7165	0.0412	0.1206
α	0.0057	0.7426	0.0010	9.15×10^{-5}
β	0.8252	1.0158	0.5248	0.5190
Ω	1.2279		0.9391	0.9369
c		0.7602		

[a]Only reactions directly affecting species densities are included in the FKM. The additional electron impact collisions such as momentum transfer and excitation of vibrational and electronic states are included in the EETM to account for the transport and energy loses of electron. Vibrational cross sections for c-C_4F_8 and C_2F_4 were analytically represented using Eqs. (5) and (6) and fitting parameters are listed on the bottom of the table.
[b]Rate coefficients have units of cm^3/s unless noted otherwise.
[c]Rate coefficient is calculated from electron energy distribution obtained in the EETM using the cross section from the cited reference.
[d]Cross section was obtained by detailed balance.
[e]Estimated by analogy to NF.
[f]Estimated by analogy to CF_4.
[g]Estimated using Maxwellian distribution.
[h]Estimated by analogy to C_2F_6.
[i]Estimated by analogy to C_2F_4.
[j]Cross section was analytically represented using Eq. (8).

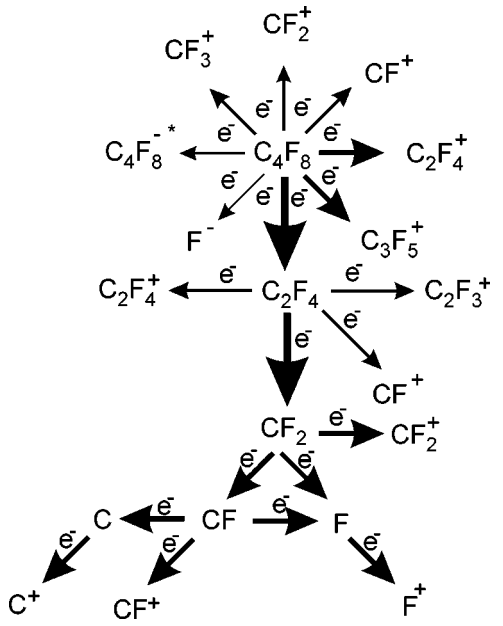

FIG. 1. Schematic of electron impact reactions in c-C_4F_8. The thickness of arrows represents the value of reaction rates calculated for an ICP at 6 mTorr, 600 W, 13.56 MHz.

co-workers[47] are consistent within the uncertainty of measurements and we chose without prejudice to use Jiao's cross sections. The branching ratios for dissociative excitation of c-C_4F_8 into neutral fragments have not been studied in detail. Following studies by Font *et al.*[14] and Rauf and Ventzek,[16] we assumed that

$$e + c\text{-}C_4F_8 \rightarrow C_2F_4 + C_2F_4 + e \tag{7}$$

is the major branching. This choice is consistent with data available for thermal and multiphoton dissociation of c-C_4F_8.[57,58] Mass spectrometry measurements of Toyoda and co-workers[56] for electron impact dissociation of c-C_4F_8 indicate minor branchings to CF, CF_2, CF_3, and C_3F_5. These processes were not included in the mechanism since their cross sections are at least an order magnitude less than the total dissociation cross section reported in Ref. 14 at energies below about 50 eV. Subsequent improvements to the model will include these branchings. The dissociation cross section for c-C_4F_8 from Ref. 14 was analytically represented using Eq. (1) and Φ for dissociative collisions was[55]

$$\Phi(E,w) = \log_{10}(4c[E/w] + e). \tag{8}$$

The fitting parameters f_0, α, β, c are listed in Table II.

Due to the large ionization and neutral dissociation cross sections of c-C_4F_8 one can expect an abundance of C_2F_4 in c-C_4F_8 plasmas. The important electron impact C_2F_4 processes include elastic collisions, vibrational excitations, dissociation, and ionization whose cross sections are shown in Fig. 2. The cross sections of these processes were largely obtained from Refs. 15 and 59. Attachment was neglected since its branching is believed to be negligibly small.[15] Vibrational excitation cross sections were analytically represented using Eq. (5) and the fitting parameters are listed in

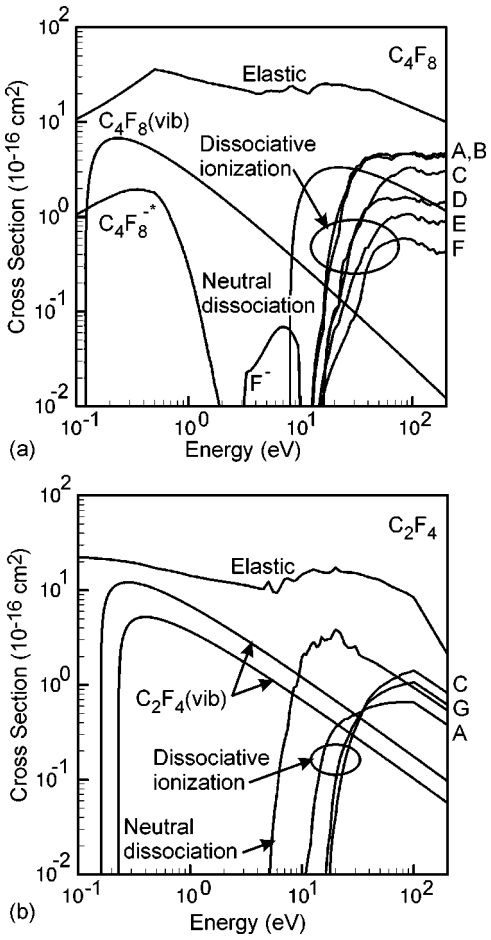

FIG. 2. Electron impact cross sections for (a) c-C_4F_8 and (b) C_2F_4. A, B, C, D, E, F, and G represent $C_2F_4^+$, $C_3F_5^+$, CF^+, CF_3^+, CF_2^+, F^+, and $C_2F_3^+$, respectively.

Table II. Since CF_2 is the most likely product channel in C_2F_4 thermal dissociation reaction, we assumed that the major branching for electron impact dissociation of C_2F_4 is[57]

$$e + C_2F_4 \rightarrow CF_2 + CF_2 + e. \tag{9}$$

Another possible branching for C_2F_4 dissociation is

$$e + C_2F_4 \rightarrow CF_3 + CF + e. \tag{10}$$

Although this channel was neglected in our initial reaction mechanism, parametric studies show that this is a critical reaction to refine the mechanism when additional experimental data became available.

B. Neutral heavy particle reactions

Neutral heavy particle reactions included in the mechanism are listed in Table III. A subset of the rate coefficients for reactions in Table III was estimated. A major class of such rate constants is for deactivation of Ar* by fluorocarbon radicals. A second class is for associative reactions of CF_x radicals, $F + CF_x + M \rightarrow CF_{x+1} + M$. As these latter reactions are not terribly important at the pressure of interest ($<$10s mTorr) uncertainty in their values is not critical.

TABLE III. Neutral heavy particle reactions.

Reaction	Rate coefficient[a]	Reference
Excitation transfer and radiative decay		
$Ar^* + O_2 \rightarrow O + O + Ar$	2.1×10^{-10}	66
$Ar^* + O \rightarrow O^* + Ar$	4.1×10^{-11}	67
$Ar^* + CF_2 \rightarrow CF + F + Ar$	6.0×10^{-11}	68[b]
$Ar^* + CF_3 \rightarrow CF_2 + F + Ar$	6.0×10^{-11}	68[b]
$Ar^* + CF_4 \rightarrow CF_2 + F_2 + Ar$	6.0×10^{-11}	68
$Ar^* + C_2F_4 \rightarrow CF_2 + CF_2 + Ar$	4.0×10^{-11}	68[b]
$Ar^* + C_2F_5 \rightarrow C_2F_5 + Ar$	4.0×10^{-11}	68[b]
$Ar^* + C_2F_6 \rightarrow CF_3 + CF_3 + Ar$	4.0×10^{-11}	68
$Ar^* + C_3F_5 \rightarrow C_3F_5 + Ar$	4.0×10^{-11}	68[b]
$Ar^* + C_3F_6 \rightarrow C_3F_6 + Ar$	4.0×10^{-11}	68[b]
$Ar^* + C_3F_7 \rightarrow C_3F_7 + Ar$	4.0×10^{-11}	68[b]
$Ar^* + C_4F_8 \rightarrow C_2F_4 + C_2F_4 + Ar$	9.0×10^{-10}	68[b]
$Ar^* + Ar^* \rightarrow Ar^+ + Ar + e$	1.2×10^{-9}	69
$Ar^{**} + Ar^{**} \rightarrow Ar^+ + Ar + e$	1.2×10^{-9}	69
$Ar^{**} + Ar^* \rightarrow Ar^+ + Ar + e$	1.2×10^{-9}	69
$Ar^{**} \rightarrow Ar^*$	$10^5\ s^{-1}$	d
$Ar^+ + Ar \rightarrow Ar^+ + Ar$	5.7×10^{-10}	70
$O^* + Ar \rightarrow O + Ar$	5.0×10^{-13}	e
$O_2^* + Ar \rightarrow O_2 + Ar$	1.0×10^{-19}	64
$O^* + O \rightarrow O + O$	8.0×10^{-12}	71
$O^* + O_2 \rightarrow O + O_2^*$	1.6×10^{-12}	72
$O^* + O_2 \rightarrow O + O_2$	4.8×10^{-12}	72
$O_2^* + O \rightarrow O_2 + O$	2.0×10^{-16}	73
$O_2^* + O_2 \rightarrow O_2 + O_2$	3.0×10^{-18}	72
$O_2^* + O_2^* \rightarrow O_2 + O_2$	9.0×10^{-17}	73[f]
$O + O + M \rightarrow O_2^* + M$	$1.9\times10^{-35}\,(T/300)^{-0.63}\ cm^6\ s^{-1}$	71
$O^* + CF_4 \rightarrow O + CF_4$	1.8×10^{-13}	g
$O^* + COF_2 \rightarrow O + COF_2$	5.3×10^{-11}	g
$O^* + COF_2 \rightarrow F_2 + CO_2$	2.1×10^{-11}	g
$O^* + CF_3 \rightarrow COF_2 + F$	3.1×10^{-11}	g
$O^* + CF_2 \rightarrow COF + F$	1.4×10^{-11}	g
$O^* + CF_2 \rightarrow CO + F + F$	4.0×10^{-12}	g
$O^* + CF \rightarrow CO + F$	2.0×10^{-11}	g
$O^* + COF \rightarrow CO_2 + F$	9.3×10^{-11}	g
$O^* + FO \rightarrow O_2 + F$	5.0×10^{-11}	g
Collisions between fluorocarbons, O, O_2, CO, COF and FO		
$O + O + M \rightarrow O_2 + M$	$2.6\times10^{-34}\,(T/300)^{-0.63}\ cm^6\ s^{-1}$	71
$O + FO \rightarrow O_2 + F$	2.7×10^{-11}	72
$O + F + M \rightarrow FO + M$	$1.0\times10^{-33}\ cm^6\ s^{-1}$	e
$C + O_2 \rightarrow CO + O$	1.6×10^{-11}	74
$CO + O + M \rightarrow CO_2 + M$	$8.3\times10^{-34}\exp(-1510/T)\ cm^6\ s^{-1}$	75
$COF + CF_2 \rightarrow CF_3 + CO$	3.0×10^{-13}	e
$COF + CF_2 \rightarrow COF_2 + CF$	3.0×10^{-13}	e
$COF + CF_3 \rightarrow CF_4 + CO$	1.0×10^{-11}	e
$COF + CF_3 \rightarrow COF_2 + CF_2$	1.0×10^{-11}	e
$COF + COF \rightarrow COF_2 + CO$	1.0×10^{-11}	e
$O + CF \rightarrow CO + F$	6.6×10^{-11}	76
$O + CF_2 \rightarrow COF + F$	3.1×10^{-11}	77
$O + CF_2 \rightarrow CO + F + F$	4.0×10^{-12}	78[e]
$O + CF_3 \rightarrow COF_2 + F$	3.3×10^{-11}	79
$O + C_2F_4 \rightarrow CF_2 + CF_2 + O$	2.7×10^{-12}	80
$O + COF \rightarrow CO_2 + F$	9.3×10^{-11}	81
$O_2 + CF \rightarrow COF + O$	3.3×10^{-11}	76
Fluorocarbon collisions		
$C + C_2F_4 \rightarrow C_2F_3 + CF$	1.91×10^{-10}	82
$CF_2 + CF_3 \rightarrow C_2F_5$	1.0×10^{-12}	83
$CF_2 + CF_2 \rightarrow C_2F_4$	7.21×10^{-14}	84
$CF_3 + CF_3 + M \rightarrow M + C_2F_6$	$3.94\times10^{-29}\ cm^6\ s^{-1}$	85
$CF_3 + CF_3 \rightarrow C_2F_6$	8.30×10^{-12}	83
$F + CF_3 \rightarrow CF_4$	2.0×10^{-11}	86
$F + CF_2 \rightarrow CF_3$	1.8×10^{-11}	87
$F + CF \rightarrow CF_2$	9.96×10^{-11}	76

TABLE III. (*Continued*).

Reaction	Rate coefficient[a]	Reference
$F+F+M \rightarrow F_2+M$	6.77×10^{-34} cm^6 s^{-1}	85
$F+C_2F_4 \rightarrow CF_3+CF_2$	4.8×10^{-11}	88
$F+C_2F_5 \rightarrow CF_3+CF_3$	1.0×10^{-11}	89
$F+C_4F_7 \rightarrow C_2F_4+C_2F_4$	1.0×10^{-11}	e
$F+C_3F_6 \rightarrow C_3F_7$	1.0×10^{-12}	89[e]
$F+C_2F_3 \rightarrow C_2F_4$	1.0×10^{-12}	89
$F+CF_3+M \rightarrow CF_4+M$	1.6×10^{-28}	88
$F_2+CF_2 \rightarrow CF_3+F$	8.3×10^{-14}	76
$F_2+CF_3 \rightarrow CF_4+F$	1.9×10^{-14}	90
$F_2+C_2F_4 \rightarrow C_2F_5+F$	3.5×10^{-16}	91
$F_2+C_3F_6 \rightarrow C_3F_7+F$	3.5×10^{-16}	91

[a]Rate coefficients have units of cm^3 s^{-1} unless noted otherwise.
[b]Estimated by analogy to CF_4.
[c]Estimated by analogy to C_2F_6.
[d]Estimated for a mildly trapped optical transition.
[e]Estimated.
[f]Estimated assuming half branching to O_2.
[g]Estimated by analogy to O.

C. Ion-neutral reactions

Ion-neutral reactions are listed in Table IV. These reactions were classified as exothermic reactions, which occur independent of ion energy, and endothermic reactions which typically have energy defects of a few eV. The exothermic processes include the vast majority of reactions which occur at all locations in the plasma. The endothermic reactions mostly occur in the sheath, where ions are accelerated to energies in excess of the energy defect. Since for our conditions the sheath is essentially collisionless, these latter processes were neglected. Ion-molecule reactions with many fluorocarbon feedstock gases and their fragments are often dissociative. For example, Ar^+ has an ionization potential 15.8 eV sufficient to produce dissociative ionization of c-C_4F_8 having a threshold of 11.5 eV. The probability of dissociative ionization between Ar^+ and CF_2 is likely to be small as CF_2 has a dissociative ionization potential of about 14 eV.

D. Ion–ion and electron-ion reactions

The rate constants of electron-ion and ion–ion reactions are listed in Table V. These reactions are important as they determine the importance of volumetric loss of ions compared to diffusion to the walls. Since negative ions are generally lost only in the volume, these rates directly determine the negative ion density. The major class of estimated reactions here is ion–ion neutralization reactions. Neither products of recombination nor reaction rates of these reactions are typically known. These reactions are fast as typical rate constants are 10^{-7} cm^3 s^{-1}. We estimated the rates of these reactions to be smaller for heavy ions and larger for lighter ions as the rate coefficient approximately scales as $\mu^{-0.5}$, where μ is the reduced mass of colliding ions.[60,61] Another important class of estimated reactions is dissociative electron-ion recombination, whose rate coefficient is typically in the range of $10^{-7}/T_e^{1/2}$ cm^3 s^{-1}, where T_e is in eV.

E. Surface reactions

We acknowledge that the dispositions of surface reactions are critical to the development of a successful reaction mechanism for the low-pressure plasmas of interest. In this work, we have employed a simple surface reaction mechanism in which all ions neutralize, returning to the plasma as their neutral counterparts and small radicals stick or react with probabilities of 0.01 for CF_2 and CF_3 to as large as 0.5 for F. This mechanism was not optimized nor parametrized to obtain better agreement with experiments, and so represents a point of departure for further studies. An exhaustive report on the investigation of surface reaction mechanisms in fluorocarbon plasmas, including c-C_4F_8, will be discussed in an upcoming publication.

IV. SPATIALLY RESOLVED PLASMA PROPERTIES, ION SATURATION CURRENTS, AND ION SPECTRA

A schematic of the reactor used in this study is shown in Fig. 3. The ICP was produced in a cylindrically symmetric chamber (13 cm in radius and 12 cm tall) using a three-turn antenna set atop a quartz window 1 cm thick. Gas was injected through the inlet below the dielectric window and was pumped out from the bottom of the reactor. A metal ring with or without permanent magnets was used to confine the plasma. Details of the reactor configuration are discussed in Paper I.[19]

Plasma properties in an ICP sustained in an Ar/c-$C_4F_8/CO/O_2=60/5/25/10$ mixture for the base case conditions (10 mTorr, 600 W, 13.56 MHz, 20 sccm) are shown in Fig. 4. This gas mixture was chosen as being representative of typical process conditions for fluorocarbon plasma etching of SiO_2. The peak electron density of 1.6×10^{11} cm^{-3} results from the drift of thermal electrons towards the peak of the plasma potential of 15 eV in the middle of reactor. The peak electron temperature of 4.3 eV

TABLE IV. Ion molecule reactions.

Reaction	Rate coefficient[a]	Reference
Charge exchange collisions		
$Ar^+ + O_2 \rightarrow O_2^+ + Ar$	5.1×10^{-11}	92
$Ar^+ + O \rightarrow O^+ + Ar$	6.4×10^{-12}	93
$Ar^+ + CF_2 \rightarrow CF^+ + Ar + F$	5.0×10^{-10}	94[b]
$Ar^+ + CF_3 \rightarrow CF_2^+ + Ar + F$	5.0×10^{-10}	94[b]
$Ar^+ + CF_4 \rightarrow CF_3^+ + Ar + F$	4.8×10^{-10}	94
$Ar^+ + C_2F_6 \rightarrow CF_3^+ + CF_3 + Ar$	5.0×10^{-10}	95[c]
$Ar^+ + C_4F_8 \rightarrow CF_3^+ + C_3F_5 + Ar$	1.0×10^{-10}	95[c]
$Ar^+ + C_4F_8 \rightarrow C_3F_5^+ + CF_3 + Ar$	3.0×10^{-10}	95[c]
$Ar^+ + C_4F_8 \rightarrow C_2F_4^+ + C_2F_4 + Ar$	3.0×10^{-10}	95[c]
$Ar^+ + C_4F_8 \rightarrow CF^+ + C_3F_7 + Ar$	1.0×10^{-10}	95[c]
$C^+ + C \rightarrow C^+ + C$	3.0×10^{-9}	14[d,e]
$C^+ + CF \rightarrow CF^+ + C$	3.18×10^{-9}	14
$CF^+ + CF \rightarrow CF^+ + CF$	1.0×10^{-9}	96[f,e]
$CF^+ + CF_2 \rightarrow CF_2^+ + CF$	1.0×10^{-9}	96[f]
$CF^+ + CF_3 \rightarrow CF_3^+ + CF$	1.71×10^{-9}	96
$CF_2^+ + CF_2 \rightarrow CF_2^+ + CF_2$	1.0×10^{-9}	14[f,e]
$CF_2^+ + CF_3 \rightarrow CF_3^+ + CF_2$	1.48×10^{-9}	14
$CF_3^+ + C_3F_5 \rightarrow C_3F_5^+ + CF_3$	7.04×10^{-10}	97
$CF_3^+ + C_3F_7 \rightarrow C_3F_7^+ + CF_3$	7.04×10^{-10}	97[g]
$CF_3^+ + CF_3 \rightarrow CF_3^+ + CF_3$	1.0×10^{-9}	14[b,e]
$C_2F_4^+ + C_2F_4 \rightarrow C_2F_4 + C_2F_4^+$	4.0×10^{-9}	e
$C_2F_5^+ + C_2F_5 \rightarrow C_2F_5 + C_2F_5^+$	4.0×10^{-9}	e
$C_3F_5^+ + C_3F_5 \rightarrow C_3F_5^+ + C_3F_5$	3.0×10^{-9}	e
$C_3F_7^+ + C_3F_7 \rightarrow C_3F_7^+ + C_3F_7$	3.0×10^{-9}	e
$C^+ + CF_3 \rightarrow CF_2^+ + CF$	2.48×10^{-9}	14
$CF^+ + CF_4 \rightarrow CF_3^+ + CF_2$	1.80×10^{-10}	98
$CF^+ + C_2F_4 \rightarrow CF_3^+ + CF + CF$	2.60×10^{-10}	97
$CF^+ + C_2F_4 \rightarrow C_3F_5^+$	1.30×10^{-10}	97
$CF^+ + C_2F_6 \rightarrow CF_3^+ + C_2F_4$	2.0×10^{-10}	98
$CF_2^+ + C_4F_8 \rightarrow C_3F_5 + C_2F_4 + F$	2.10×10^{-11}	14
$CF_2^+ + C_2F_4 \rightarrow C_2F_4^+ + CF_2$	1.00×10^{-9}	97
$CF_2^+ + C_2F_6 \rightarrow C_2F_5^+ + CF_3$	3.50×10^{-11}	14, 99
$CF_2^+ + CF_4 \rightarrow CF_3^+ + CF_3$	0.40×10^{-9}	98
$CF_2^+ + CF \rightarrow CF_3^+ + C$	2.06×10^{-9}	14
$CF_2^+ + C \rightarrow CF^+ + CF$	1.04×10^{-9}	14
$CF_3^+ + C_2F_4 \rightarrow C_3F_7^+$	3.30×10^{-11}	97
$CF_3^+ + C_2F_6 \rightarrow C_2F_5^+ + CF_4$	2.50×10^{-12}	98
$CF_3^- + F \rightarrow CF_3 + F^-$	5.0×10^{-8}	100
$CF_3^- + CF_3 \rightarrow C_2F_6 + e$	1.0×10^{-10}	k
$C_2F_4^+ + C_2F_4 \rightarrow C_3F_5^+ + CF_3$	2.0×10^{-11}	97
$C_3F_7^+ + C_2F_4 \rightarrow CF_3^+ + C_4F_8$	2.0×10^{-11}	97
$C_4F_8^- + F \rightarrow C_4F_8 + F^-$	1.0×10^{-9}	k
$CO^+ + C_2F_4 \rightarrow C_2F_4^+ + CO$	1.10×10^{-9}	99
$CO^+ + C_3F_6 \rightarrow C_3F_6^+ + CO$	7.31×10^{-10}	99
$CO^+ + O \rightarrow O^+ + CO$	1.40×10^{-10}	101
$CO^+ + CF_2 \rightarrow CF^+ + COF$	7.0×10^{-10}	101[d]
$CO^+ + CF_3 \rightarrow CF_2^+ + COF$	7.0×10^{-10}	101[d]
$CO^+ + CF_4 \rightarrow CF_3^+ + COF$	7.0×10^{-10}	101
$CO^+ + C_3F_6 \rightarrow C_2F_4^+ + CF_2 + CO$	4.76×10^{-10}	99
$CO^+ + C_3F_6 \rightarrow C_3F_5^+ + F + CO$	4.93×10^{-10}	99
$CO^+ + C_4F_8 \rightarrow C_3F_5^+ + CF_3 + CO$	4.86×10^{-10}	99[h]
$CO^+ + C_4F_8 \rightarrow C_3F_6^+ + CF_2 + CO$	4.68×10^{-10}	99[h]
$CO^+ + C_4F_8 \rightarrow C_4F_7^+ + F + CO$	7.02×10^{-10}	99[h]
$CO^+ + C_2F_6 \rightarrow CF_3^+ + CF_3 + CO$	4.51×10^{-10}	99
$CO^+ + C_2F_6 \rightarrow C_2F_5^+ + F + CO$	6.49×10^{-10}	99
$CO^+ + O_2 \rightarrow O_2^+ + CO$	1.20×10^{-10}	101
$CO^+ + C_4F_8 \rightarrow C_4F_8^+ + CO$	1.44×10^{-10}	99
$F^+ + O \rightarrow O^+ + F$	1.0×10^{-10}	102
$F^+ + O_2 \rightarrow O_2^+ + F$	7.14×10^{-10}	102
$F^+ + F \rightarrow F^+ + F$	1.0×10^{-9}	14[e,i]
$F^+ + F_2 \rightarrow F_2^+ + F$	7.94×10^{-10}	14
$F^+ + C \rightarrow C^+ + F$	1.17×10^{-9}	14
$F^+ + CF \rightarrow C^+ + F_2$	2.71×10^{-9}	14
$F^+ + CF_2 \rightarrow CF^+ + F_2$	2.28×10^{-9}	14
$F^+ + CF_3 \rightarrow CF_2^+ + F_2$	2.90×10^{-9}	14

TABLE IV. (*Continued*).

Reaction	Rate coefficient[a]	Reference
$F^+ + CF_4 \rightarrow CF_3^+ + F_2$	1.0×10^{-9}	14
$F^+ + C_2F_4 \rightarrow C_2F_3^+ + F_2$	1.0×10^{-9}	14
$F^+ + C_2F_6 \rightarrow C_2F_5^+ + F_2$	1.0×10^{-9}	14
$F^+ + C_2F_5 \rightarrow C_2F_4^+ + F_2$	1.0×10^{-9}	14
$F^+ + O_2 \rightarrow O^+ + FO$	5.04×10^{-11}	102
$F_2^+ + CF \rightarrow CF_2^+ + F$	2.18×10^{-9}	14
$F_2^+ + C \rightarrow CF^+ + F$	1.04×10^{-9}	14
$F_2^+ + CF_2 \rightarrow CF_3^+ + F$	1.79×10^{-9}	14
$F_2^+ + CF_3 \rightarrow CF_3^+ + F + F$	1.60×10^{-9}	14
$F_2^+ + CF_4 \rightarrow CF_3^+ + F + F_2$	1.0×10^{-10}	14[k]
$F_2^+ + C_2F_4 \rightarrow C_2F_4^+ + F_2$	1.0×10^{-10}	14[k]
$F_2^+ + C_2F_5 \rightarrow C_2F_5^+ + F_2$	1.0×10^{-10}	14[k]
$F_2^+ + F_2 \rightarrow F_2^+ + F_2$	1.0×10^{-9}	e,k
$O + O^+ \rightarrow O^+ + O$	1.0×10^{-9}	71[e]
$O^+ + C_2F_4 \rightarrow C_2F_4^+ + O$	1.30×10^{-9}	99
$O^+ + C_3F_6 \rightarrow C_3F_6^+ + O$	1.24×10^{-9}	99
$O^+ + C_4F_8 \rightarrow C_4F_8^+ + O$	1.22×10^{-9}	99
$O_2^+ + C_2F_4 \rightarrow C_2F_4^+ + O_2$	9.80×10^{-10}	99
$O_2^+ + C_2F_5 \rightarrow C_2F_5^+ + O_2$	1.0×10^{-9}	99[j]
$O_2^+ + C_3F_6 \rightarrow C_3F_6^+ + O_2$	1.08×10^{-9}	99
$O_2^+ + C_4F_8 \rightarrow C_4F_8^+ + O_2$	1.55×10^{-9}	99
$O_2^- + F \rightarrow O_2 + F^-$	1.0×10^{-7}	k
$O_2^+ + O_2 \rightarrow O_2 + O_2^+$	1.0×10^{-9}	101
$O_2^- + O \rightarrow O^- + O_2$	1.50×10^{-10}	101
$O^+ + O_2 \rightarrow O_2^+ + O$	1.0×10^{-11}	101
$O^+ + CF_4 \rightarrow CF_3^+ + FO$	1.40×10^{-9}	46
$O^+ + C_2F_6 \rightarrow C_2F_5^+ + F + O$	1.30×10^{-10}	99
$O^+ + C_2F_6 \rightarrow CF_3^+ + CF_3 + O$	1.47×10^{-9}	99
$O^+ + C_3F_6 \rightarrow C_2F_4^+ + CF_2 + O$	0.29×10^{-9}	99
$O^+ + C_3F_6 \rightarrow C_3F_5^+ + F + O$	0.38×10^{-9}	99
$O^+ + C_4F_8 \rightarrow C_3F_5^+ + CF_3 + O$	0.76×10^{-9}	99
$O^+ + C_4F_8 \rightarrow C_4F_7^+ + F + O$	0.28×10^{-9}	99
$O_2^+ + CF_4 \rightarrow CF_3^+ + O_2 + F$	$8.45\times10^{-17}\,(T/300)^{1.2}\times\exp(-41{,}739/T)$	103
$O_2^+ + C_2F_6 \rightarrow CF_3^+ + CF_3 + O_2$	$3.03\times10^{-17}\,(T/300)^{1.4}\times\exp(-34{,}783/T)$	103
$O_2^+ + C_2F_6 \rightarrow C_2F_5^+ + F + O_2$	$7.88\times10^{-14}\,(T/300)^{1.9}\times\exp(-34{,}783/T)$	103
$O_2^+ + C_3F_6 \rightarrow C_2F_4^+ + CF_2 + O_2$	0.18×10^{-9}	99
$O_2^+ + C_3F_6 \rightarrow C_3F_5^+ + F + O_2$	0.14×10^{-9}	99
$O_2^+ + C_4F_8 \rightarrow C_2F_4^+ + C_2F_4 + O_2$	4.48×10^{-10}	46[h]
$O_2^+ + C_4F_8 \rightarrow C_3F_5^+ + CF_3 + O_2$	1.15×10^{-9}	46[h]
$O + O^+ + M \rightarrow O_2^+ + M$	1.0×10^{-29}	71
$O_2^- + C_4F_8 \rightarrow C_4F_8^- + O_2$	4.60×10^{-10}	46
$O^- + C_4F_8 \rightarrow O + C_4F_8^-$	1.0×10^{-10}	46[k]
Ion neutralization and ion deactivation collisions		
$C_4F_8^{-*} \rightarrow C_4F_8 + e$	$2.0\times10^{6}\ s^{-1}$	51, 52
$C_4F_8^{-*} + M \rightarrow C_4F_8^- + M$	1.0×10^{-10}	k
$F^- + CF_3 \rightarrow CF_4 + e$	4.0×10^{-10}	13
$F^- + CF_2 \rightarrow CF_3 + e$	3.0×10^{-10}	13
$F^- + CF \rightarrow CF_2 + e$	2.0×10^{-10}	13
$F^- + C \rightarrow CF + e$	1.0×10^{-10}	13
$F^- + F \rightarrow F_2 + e$	1.0×10^{-10}	13
$F^- + O \rightarrow F + O + e$	1.0×10^{-10}	13
$O_2^- + O_2^* \rightarrow e + O_2 + O_2$	2.0×10^{-10}	101
$O^- + O \rightarrow O_2 + e$	2.0×10^{-10}	101

[a]Rate coefficients have units of $cm^3\,s^{-1}$ unless noted otherwise. Two body rate coefficients are shown for $T=330$ K and are scaled by $(T/300)^{1/2}$.
[b]Estimated by analogy to CF_4.
[c]Calculated from cross sections using Maxwell distribution.
[d]Estimated by analogy to CF.
[e]Included for gas heating only.
[f]Estimated by analogy to CF_3.
[g]Estimated by analogy to C_3F_5.
[h]Estimated by analogy to $2-C_4F_8$.
[i]Estimated by analogy to F_2.
[j]Estimated by analogy to C_2F_4.
[k]Estimated.

TABLE V. Ion–ion and ion-electron reactions.

Reaction	Rate coefficient[a]	Reference
Ion–ion neutralization		
$CF_3^- + Ar^+ \rightarrow CF_3 + Ar$	2.0×10^{-7}	104
$CF_3^- + O_2^+ \rightarrow CF_3 + O_2$	2.0×10^{-7}	60, 61[b]
$CF_3^- + O^+ \rightarrow CF_3 + O$	2.5×10^{-7}	60, 61[b]
$CF_3^- + CO^+ \rightarrow CF_3 + CO$	2.0×10^{-7}	60, 61[b]
$CF_3^- + CF^+ \rightarrow CF_3 + CF$	2.0×10^{-7}	60, 61[b]
$CF_3^- + C^+ \rightarrow CF_3 + C$	3.0×10^{-7}	60, 61[b]
$CF_3^- + F^+ \rightarrow CF_3 + F$	2.5×10^{-7}	60, 61[b]
$CF_3^- + F_2^+ \rightarrow CF_3 + F_2$	2.0×10^{-7}	60, 61[b]
$CF_3^- + CF_3^+ \rightarrow CF_3 + CF_3$	1.5×10^{-7}	104
$CF_3^- + C_2F_4^+ \rightarrow CF_3 + C_2F_4$	1.0×10^{-7}	60, 61[b]
$CF_3^- + C_2F_3^+ \rightarrow CF_3 + C_2F_3$	1.0×10^{-7}	60, 61[b]
$CF_3^- + C_2F_5^+ \rightarrow CF_3 + C_2F_5$	1.0×10^{-7}	60, 61[b]
$CF_3^- + C_3F_5^+ \rightarrow CF_3 + C_3F_5$	1.0×10^{-7}	60, 61[b]
$CF_3^- + C_3F_7^+ \rightarrow CF_3 + C_3F_7$	1.0×10^{-7}	60, 61[b]
$CF_3^- + C_4F_7^+ \rightarrow CF_3 + C_4F_7$	1.0×10^{-7}	60, 61[b]
$CF_3^- + CF_2^+ \rightarrow CF_3 + CF_2$	2.0×10^{-7}	60, 61[b]
$C_4F_8^- + Ar^+ \rightarrow C_4F_8 + Ar$	9.0×10^{-8}	60, 61[b]
$C_4F_8^{-*} + Ar^+ \rightarrow C_4F_8 + Ar$	9.0×10^{-8}	60, 61[b]
$C_4F_8^{-*} + CO^+ \rightarrow C_4F_8 + CO$	2.0×10^{-7}	60, 61[b]
$C_4F_8^{-*} + O_2^+ \rightarrow C_4F_8 + O_2$	2.0×10^{-7}	60, 61[b]
$C_4F_8^{-*} + O^+ \rightarrow C_4F_8 + O$	2.5×10^{-7}	60, 61[b]
$C_4F_8^- + CO^+ \rightarrow C_4F_8 + CO$	2.0×10^{-7}	60, 61[b]
$C_4F_8^- + O_2^+ \rightarrow C_4F_8 + O_2$	2.0×10^{-7}	60, 61[b]
$C_4F_8^- + O^+ \rightarrow C_4F_8 + O$	2.5×10^{-7}	60, 61[b]
$C_4F_8^- + CF^+ \rightarrow C_4F_8 + CF$	1.5×10^{-7}	60, 61[b]
$C_4F_8^- + C^+ \rightarrow C_4F_8 + C$	3.0×10^{-7}	60, 61[b]
$C_4F_8^- + F^+ \rightarrow C_4F_8 + F$	2.0×10^{-7}	60, 61[b]
$C_4F_8^- + F_2^+ \rightarrow C_4F_8 + F_2$	1.5×10^{-7}	60, 61[b]
$C_4F_8^- + CF_3^+ \rightarrow C_4F_8 + CF_3$	1.0×10^{-7}	60, 61[b]
$C_4F_8^- + C_2F_4^+ \rightarrow C_4F_8 + C_2F_4$	9.0×10^{-8}	60, 61[b]
$C_4F_8^- + C_2F_3^+ \rightarrow C_4F_8 + C_2F_3$	9.0×10^{-8}	60, 61[b]
$C_4F_8^- + C_2F_5^+ \rightarrow C_4F_8 + C_2F_5$	9.0×10^{-8}	60, 61[b]
$C_4F_8^- + C_3F_5^+ \rightarrow C_4F_8 + C_3F_5$	9.0×10^{-8}	60, 61[b]
$C_4F_8^- + C_3F_6^+ \rightarrow C_4F_8 + C_3F_6$	9.0×10^{-8}	60, 61[b]
$C_4F_8^- + C_3F_7^+ \rightarrow C_4F_8 + C_3F_7$	9.0×10^{-8}	60, 61[b]
$C_4F_8^- + C_4F_7^+ \rightarrow C_4F_8 + C_4F_7$	9.0×10^{-8}	60, 61[b]
$C_4F_8^- + CF_2^+ \rightarrow C_4F_8 + CF_2$	1.0×10^{-7}	60, 61[b]
$C_4F_8^{-*} + CF^+ \rightarrow C_4F_8 + CF$	2.0×10^{-7}	60, 61[b]
$C_4F_8^{-*} + C^+ \rightarrow C_4F_8 + C$	3.0×10^{-7}	60, 61[b]
$C_4F_8^{-*} + F^+ \rightarrow C_4F_8 + F$	2.0×10^{-7}	60, 61[b]
$C_4F_8^{-*} + F_2^+ \rightarrow C_4F_8 + F_2$	1.5×10^{-7}	60, 61[b]
$C_4F_8^{-*} + CF_3^+ \rightarrow C_4F_8 + CF_3$	1.0×10^{-7}	60, 61[b]
$C_4F_8^{-*} + C_2F_4^+ \rightarrow C_4F_8 + C_2F_4$	9.0×10^{-8}	60, 61[b]
$C_4F_8^{-*} + C_2F_3^+ \rightarrow C_4F_8 + C_2F_3$	9.0×10^{-8}	60, 61[b]
$C_4F_8^{-*} + C_2F_5^+ \rightarrow C_4F_8 + C_2F_5$	9.0×10^{-8}	60, 61[b]
$C_4F_8^{-*} + C_3F_5^+ \rightarrow C_4F_8 + C_3F_5$	9.0×10^{-8}	60, 61[b]
$C_4F_8^{-*} + C_3F_6^+ \rightarrow C_4F_8 + C_3F_6$	9.0×10^{-8}	60, 61[b]
$C_4F_8^{-*} + C_3F_7^+ \rightarrow C_4F_8 + C_3F_7$	9.0×10^{-8}	60, 61[b]
$C_4F_8^{-*} + C_4F_7^+ \rightarrow C_4F_8 + C_4F_7$	9.0×10^{-8}	60, 61[b]
$C_4F_8^{-*} + CF_2^+ \rightarrow C_4F_8 + CF_2$	1.0×10^{-7}	60, 61[b]
$F^- + Ar^+ \rightarrow F + Ar$	2.0×10^{-7}	104
$F^- + O_2^+ \rightarrow F + O_2$	3.0×10^{-7}	13
$F^- + CO^+ \rightarrow F + CO$	3.0×10^{-7}	13
$F^- + O^+ \rightarrow F + O$	3.0×10^{-7}	13
$F^- + CF_3^+ \rightarrow F + CF_3$	8.7×10^{-8}	14
$F^- + CF_2^+ \rightarrow F + CF_2$	9.1×10^{-8}	14
$F^- + CF^+ \rightarrow CF + F$	9.8×10^{-8}	14
$F^- + F_2^+ \rightarrow F + F_2$	9.4×10^{-8}	14
$F^- + F^+ \rightarrow F + F$	3.1×10^{-7}	14
$F^- + C^+ \rightarrow F + C$	2.2×10^{-7}	14
$F^- + C_2F_5^+ \rightarrow F + C_2F_5$	9.0×10^{-8}	60, 61[b]
$F^- + C_2F_3^+ \rightarrow F + C_2F_3$	9.0×10^{-8}	60, 61[b]

TABLE V. (*Continued*).

Reaction	Rate coefficient[a]	Reference
$F^- + CF_3^+ \rightarrow CF_2 + F_2$	8.7×10^{-8}	14
$F^- + CF_3^+ \rightarrow CF_2 + F + F$	3.0×10^{-7}	13
$F^- + CF_2^+ \rightarrow CF + F_2$	9.1×10^{-8}	14
$F^- + CF^+ \rightarrow C + F + F$	4.0×10^{-7}	13
$F^- + C_2F_4^+ \rightarrow CF + CF_2 + F_2$	8.2×10^{-8}	14
$F^- + C_3F_5^+ \rightarrow C_2F_4 + CF_2$	8.0×10^{-8}	14
$F^- + C_3F_6^+ \rightarrow C_2F_4 + CF_3$	8.0×10^{-8}	14[c]
$F^- + C_3F_7^+ \rightarrow C_2F_6 + CF_2$	8.0×10^{-8}	14[c]
$F^- + C_4F_7^+ \rightarrow C_2F_5 + CF_2$	8.0×10^{-8}	14[c]
$O^- + F^+ \rightarrow O + F$	3.0×10^{-7}	60, 61[b]
$O^- + Ar^+ \rightarrow O + Ar$	3.0×10^{-7}	60, 61[b]
$O^- + O_2^+ + M \rightarrow O + O_2 + M$	$2.0\times10^{-25}\,(T/300)^{-2.5}\ \mathrm{cm^6\ s^{-1}}$	71
$O^- + O^+ + M \rightarrow O + O + M$	$2.0\times10^{-25}\,(T/300)^{-2.5}\ \mathrm{cm^6\ s^{-1}}$	71
$O^- + CF_3^+ \rightarrow O + CF_3$	2.0×10^{-7}	60, 61[b]
$O^- + C_2F_4^+ \rightarrow O + C_2F_4$	1.0×10^{-7}	60, 61[b]
$O^- + C_2F_3^+ \rightarrow O + C_2F_3$	1.0×10^{-7}	60, 61[b]
$O^- + C_2F_5^+ \rightarrow O + C_2F_5$	1.0×10^{-7}	60, 61[b]
$O^- + C_3F_5^+ \rightarrow O + C_3F_5$	1.0×10^{-7}	60, 61[b]
$O^- + C_3F_6^+ \rightarrow O + C_3F_6$	1.0×10^{-7}	60, 61[b]
$O^- + C_3F_7^+ \rightarrow O + C_3F_7$	1.0×10^{-7}	60, 61[b]
$O^- + C_4F_7^+ \rightarrow O + C_4F_7$	1.0×10^{-7}	60, 61[b]
$O^- + C_4F_8^+ \rightarrow O + C_4F_8$	1.0×10^{-7}	60, 61[b]
$O^- + CF_2^+ \rightarrow O + CF_2$	2.0×10^{-7}	60, 61[b]
$O^- + CO^+ \rightarrow O + CO$	2.0×10^{-7}	60, 61[b]
$O^- + O_2^+ \rightarrow O + O_2$	2.0×10^{-7}	71
$O^- + CF^+ \rightarrow O + CF$	2.0×10^{-7}	60, 61[b]
$O^- + C^+ \rightarrow O + C$	3.0×10^{-7}	60, 61[b]
$O^- + F^+ \rightarrow O + F$	2.0×10^{-7}	60, 61[b]
$O^- + F_2^+ \rightarrow O + F_2$	1.5×10^{-7}	60, 61[b]
$O_2^- + O_2^+ \rightarrow O_2 + O_2$	2.0×10^{-7}	71
$O_2^- + O^+ \rightarrow O_2 + O$	2.0×10^{-7}	71
$O_2^- + Ar^+ \rightarrow O_2 + Ar$	1.0×10^{-7}	60, 61[b]
$O_2^- + CF^+ \rightarrow O_2 + CF$	2.0×10^{-7}	60, 61[b]
$O_2^- + C^+ \rightarrow O_2 + C$	2.5×10^{-7}	60, 61[b]
$O_2^- + F^+ \rightarrow O_2 + F$	2.0×10^{-7}	60, 61[b]
$O_2^- + F_2^+ \rightarrow O_2 + F_2$	1.5×10^{-7}	60, 61[b]
$O_2^- + CF_3^+ \rightarrow O_2 + CF_3$	1.0×10^{-7}	60, 61[b]
$O_2^- + C_2F_4^+ \rightarrow O_2 + C_2F_4$	1.0×10^{-7}	60, 61[b]
$O_2^- + C_2F_3^+ \rightarrow O_2 + C_2F_3$	1.0×10^{-7}	60, 61[b]
$O_2^- + C_2F_5^+ \rightarrow O_2 + C_2F_5$	1.0×10^{-7}	60, 61[b]
$O_2^- + C_3F_5^+ \rightarrow O_2 + C_3F_5$	1.0×10^{-7}	60, 61[b]
$O_2^- + C_3F_6^+ \rightarrow O_2 + C_3F_6$	1.0×10^{-7}	60, 61[b]
$O_2^- + C_3F_7^+ \rightarrow O_2 + C_3F_7$	1.0×10^{-7}	60, 61[b]
$O_2^- + C_3F_6^+ \rightarrow O_2 + C_3F_6$	1.0×10^{-7}	60, 61[b]
$O_2^- + C_4F_7^+ \rightarrow O_2 + C_4F_7$	1.0×10^{-7}	60, 61[b]
$O_2^- + C_4F_8^+ \rightarrow O_2 + C_4F_8$	1.0×10^{-7}	60, 61[b]
$O_2^- + CF_2^+ \rightarrow O_2 + CF_2$	1.0×10^{-7}	60, 61[b]
$O_2^- + CO^+ \rightarrow O_2 + CO$	1.0×10^{-7}	60, 61[b]
$O_2^- + O_2^+ \rightarrow O_2 + O_2$	1.0×10^{-7}	71
$O^- + O_2^+ \rightarrow O + O + O$	1.0×10^{-7}	71
$O^- + CF^+ \rightarrow O + CF$	1.0×10^{-7}	71
Electron-ion recombination reactions		
$e + Ar \rightarrow Ar^{**}$	$8.15\times10^{-13}\,T_e^{-0.5}$	105
$e + O_2^+ \rightarrow O + O$	$1.20\times10^{-8}\,T_e^{-0.7}$	71
$e + O_2^+ \rightarrow O^* + O$	$8.88\times10^{-9}\,T_e^{-0.7}$	71
$e + O^+ \rightarrow O^*$	$5.3\times10^{-13}\,T_e^{-0.5}$	105
$e + F_2^+ \rightarrow F + F$	$8.0\times10^{-8}\,T_e^{-0.5}$	d
$e + CF^+ \rightarrow C + F$	$8.0\times10^{-8}\,T_e^{-0.5}$	d
$e + CF_3^+ \rightarrow CF_2 + F$	$8.0\times10^{-8}\,T_e^{-0.5}$	d
$e + CF_2^+ \rightarrow CF + F$	$8.5\times10^{-8}\,T_e^{-0.5}$	d
$e + C_2F_5^+ \rightarrow CF_3 + CF_2$	$8.0\times10^{-8}\,T_e^{-0.5}$	d
$e + C_2F_4^+ \rightarrow CF_2 + CF_2$	$8.0\times10^{-8}\,T_e^{-0.5}$	d
$e + C_2F_3^+ \rightarrow CF_2 + CF$	$8.0\times10^{-8}\,T_e^{-0.5}$	d

TABLE V. (*Continued*).

Reaction	Rate coefficient[a]	Reference
$e+C_3F_5^+ \rightarrow C_2F_3+CF_2$	$8.0\times10^{-8}\,T_e^{-0.5}$	d
$e+C_3F_6^+ \rightarrow C_2F_4+CF_2$	$8.0\times10^{-8}\,T_e^{-0.5}$	d
$e+C_3F_7^+ \rightarrow C_2F_4+CF_3$	$8.0\times10^{-8}\,T_e^{-0.5}$	d
$e+C_4F_7^+ \rightarrow C_2F_4+C_2F_3$	$8.0\times10^{-8}\,T_e^{-0.5}$	d

[a]Rate coefficients have units of cm^3/s unless noted otherwise. Two body rate coefficients for heavy particle collisions are shown for $T=330$ K and are scaled by $(T/300)^{1/2}$.
[b]Estimated using scaling discussed in Refs. 60 and 61 and present ion saturation current measurements.
[c]Estimated by analogy to $C_3F_5^+$.
[d]Estimated.

occurs in the middle of electromagnetic skin layer (2 cm for the base case conditions) where the power deposition peaks. The electron temperature is lower in the bulk plasma where electrons expend energy in inelastic collisions with neutrals. Ar^+ is the dominant ion for these conditions. Approaching the substrate, $[Ar^+]$ is more uniformly distributed in space than in the middle of reactor where the density of positive ions follows that of negative ions, as discussed below. The effective temperature of Ar^+, which is the sum of thermal and directed energies, is above 1 eV near the walls where ions are accelerated by the pre-sheath electric field and below 0.1 eV in the middle of the reactor as a result of ion-neutral elastic and charge exchange collisions.

$[CF^+]$, $[CF_2^+]$, $[C_2F_4^+]$, and $[F^-]$, which represent the major fluorocarbon positive and negative ions are shown in Fig. 5. The dominant negative ion F^- has its highest density of $8.5\times10^{10}\,cm^{-3}$ near the edge of skin layer where the dissociative attachment process and plasma potential peak. Positive ions are more uniformly distributed in space near the wafer than in the middle of reactor where by charge neutrality requirements they follow the density profile of negative ions. For these conditions, the concentrations of heavy positive ions are larger than or commensurate with those of light positive ions. For example, $[C_2F_4^+]$ peaks at $3\times10^{10}\,cm^{-3}$, whereas $[CF^+]$ and $[CF_2^+]$ peak at 2.2×10^{10} and $2.8\times10^{10}\,cm^{-3}$, respectively. We found that the ratio of heavy ion densities to light ion densities is sensitive to both the branching ratios for neutral dissociation and the rates of charge exchange reactions of fluorocarbon neutral

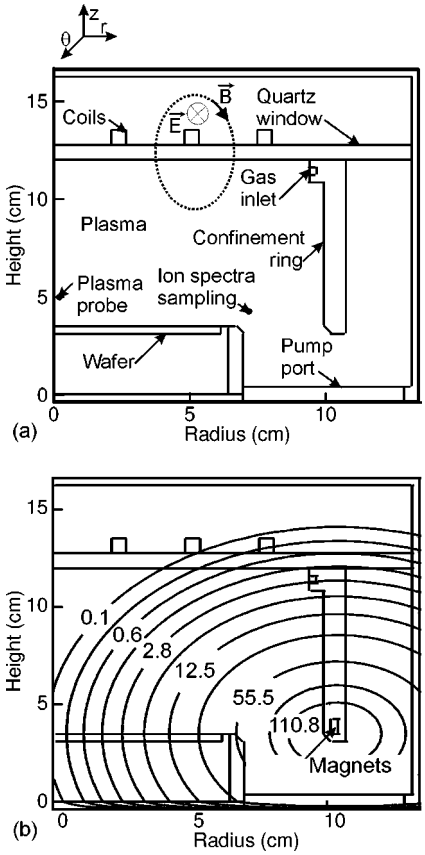

FIG. 3. Schematic of the ICP reactor (a) and radial static magnetic fields produced by permanent magnets (b). Magnetic fields produce plasma confinement by reducing diffusion losses.

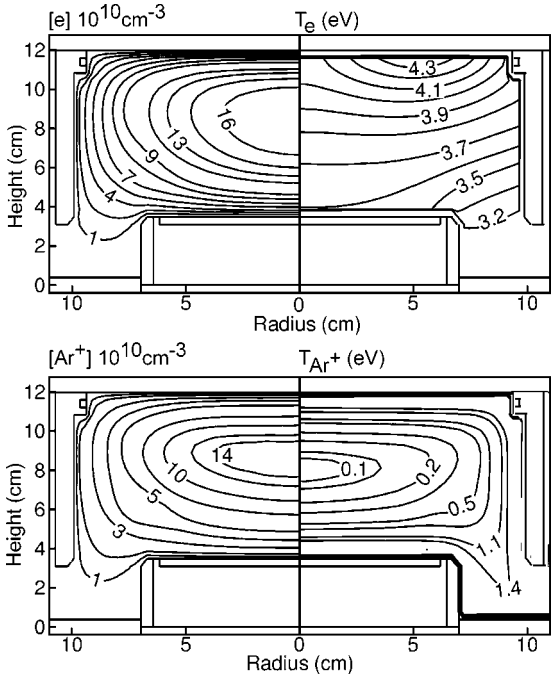

FIG. 4. Plasma parameters in an ICP sustained in Ar/c-$C_4F_8/O_2/CO = 60/10/5/25$ for the base case conditions (10 mTorr, 600 W, 13.56 MHz, 20 sccm). [e] and $[Ar^+]$ peak near the maximum in plasma potential. The electron temperature has a maximum in the skin layer where the power deposition peaks, whereas the effective ion temperature is large near the walls due the acceleration of ion by the pre-sheath electric field.

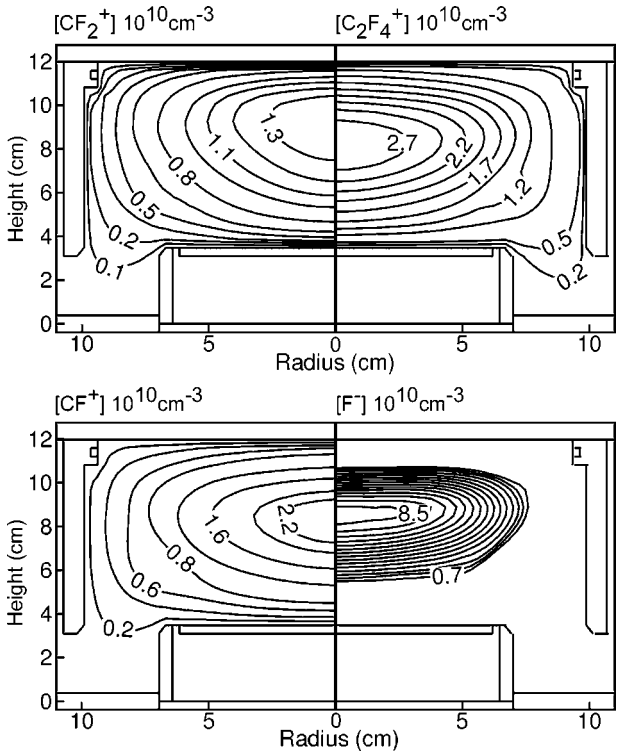

FIG. 5. Plasma parameters in an ICP sustained in $Ar/c\text{-}C_4F_8/O_2/CO = 60/10/5/25$ for the base case conditions. Positive ions are uniformly distributed in the radial direction near the wafer where the static magnetic fields produce confinement in the electron density. The density of light CF^+ follows $[F^-]$ in the center of the reactor.

species with $[Ar^+]$ and $[CO^+]$. For example, the neglect of charge exchange reactions involving light fluorocarbons such as

$$Ar^+ + CF_2 \rightarrow CF^+ + F + Ar, \tag{11}$$

$$CO^+ + CF_2 \rightarrow CF^+ + F + CO, \tag{12}$$

$$Ar^+ + CF_3 \rightarrow CF_2^+ + F + Ar, \tag{13}$$

$$CO^+ + CF_3 \rightarrow CF_2^+ + F + CO, \tag{14}$$

whose reaction rates have not been reported in the literature, results in the concentrations of heavy ions such as $C_2F_4^+$ and $C_3F_5^+$ being an order of magnitude larger than the concentration of light ions such as CF^+, CF_2^+, and CF_3^+. As these reactions are energetically allowed and so likely, we included them with estimated rate coefficients. The final disposition of the reaction mechanism requires resolution of the cracking pattern of c-C_4F_8 and C_2F_4, which in large part determines the proportion of CF_x radicals, and the relative importance of these charge exchange events.

The distributions of positive ions in part reflect their formation channels. For example, the peak density of CF_2^+ is shifted towards the top of the reactor where its source function by electron impact is largest. The CF_2^+ density is rapidly depleted by charge exchange reactions with c-C_4F_8 and C_2F_4 and so does not survive to drift to the peak of plasma potential. $C_2F_4^+$, a species which due its low ionization potential is largely consumed in the volume by electron-ion recombination or ion–ion neutralization, survives to drift to the peak of the plasma potential.

We also found that plasma properties in the center of the reactor, where electron and dominant positive ion densities peak, are sensitive to the rate of the autodetachment of $C_4F_8^-*$

$$C_4F_8^-* \rightarrow C_4F_8 + e. \tag{15}$$

For example, if the rate of this autodetachment reaction is $<10^6\,s^{-1}$ a large peak of $[C_4F_8^-*]$ occurs in the center of the reactor at the maximum of the plasma potential, a situation which we judged as being unphysical. As the highly peaked spatial profile of $C_4F_8^-*$ is partially due to the low mobility of $C_4F_8^-*$, the peak of $[C_4F_8^-*]$ could perhaps be reduced by including charge exchange reactions of $C_4F_8^-*$ with the light fluorocarbon ions, which have higher mobility and, consequently, are distributed more uniformly over the plasma area. However, the rates of such reactions are unknown and are difficult to estimate. Our rate of autodetachment was chosen rapid enough to avoid highly peaked distributions of $[C_4F_8^-*]$. The peak of $[C_4F_8^-*]$ weakly depends on the stabilization reaction

$$C_4F_8^-* + M \rightarrow C_4F_8^- + M \tag{16}$$

as even with a rate coefficient of $10^{-10}\,cm^3\,s^{-1}$ its net rate of stabilization is small. Also, this reaction does not greatly affect the distortion of plasma properties as the mobility of $C_4F_8^-$ is likely to be similar to that of $C_4F_8^-*$.

$[C_4F_8]$, $[CF_2]$, $[C_2F_4]$, and $[F]$, which represent the dominant heavy and light fluorocarbon neutral species, are shown in Fig. 6. $[C_4F_8]$ has a maximum at the inlet nozzle and a minimum at the edge of skin layer where c-C_4F_8 dissociates into C_2F_4, thereby producing a peak in $[C_2F_4]$ of $1.1\times10^{13}\,cm^{-3}$. $[C_2F_4]$ also has a large source at the walls due to the recombination of the abundant $C_2F_4^+$ fluxes. $[CF_2]$ peaks near the edge of the skin layer at $1.7\times10^{13}\,cm^{-3}$ as a consequence of C_2F_4 dissociation. It also has both sinks (due to the deposition) and sources (due to the recombination of CF_2^+) at the walls. $[CF_2]$ and $[C_2F_4]$ decrease with distance from the coils as a result of decreased dissociation of c-C_4F_8 and depletion by gas flow out of the reactor through the annulus between the substrate and confinement ring. The sourcing of CF_2 and C_2F_4 by recombination of their ions on surfaces exceeds their depletion by pumping through the annulus. There is a substantial recirculation of CF_2 and C_2F_4 from the volume to surfaces and back by this mechanism. F, being less reactive on walls and having a small ion density, is lost dominantly by pumping, and so $[F]$ monotonically decreases from the center of the reactor to the pump port.

The model was validated by comparing calculated and measured ion saturation currents for ICPs sustained in Ar, O_2, Ar/c-C_4F_8, and O_2/c-C_4F_8 with and without static magnetic fields. (The static magnetic fields are produced by the magnets shown in Fig. 3(b).) Calculated ion probe currents for ICPs sustained in Ar with magnets are compared to experiments in Fig. 7 for 10 mTorr, powers of 400 W, 600 W

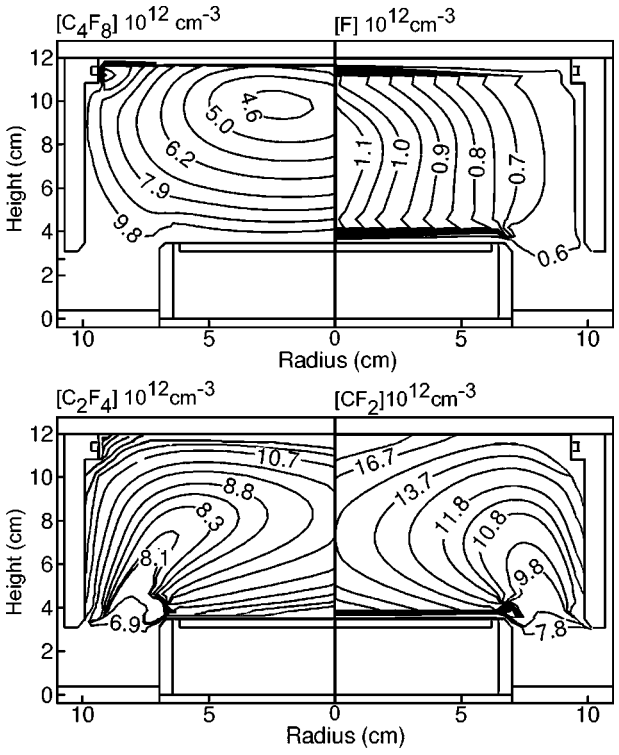

FIG. 6. Density of neutrals in an ICP sustained in Ar/c-C_4F_8/O_2/CO = 60/10/5/25 for the base case conditions. [C_4F_8] is small, and [C_2F_4] and [CF_2] are large in the skin layer as a result of electron impact dissociation. [F] peaks in the center of the reactor near the peak electron density.

and 1 kW, and probe voltages of −100 to 0 V. The probe was located on axis, ≈1 cm from the substrate. The experimental ion current was obtained by subtracting out electron current from the total probe current, whereas ion current from the model was computed using Eq. (1).

The ion saturation currents are sensitive to probe voltage due to the finite ratio of the sheath thickness to the probe radius. The ion currents approach their saturation values with decreasing (more negative) probe voltage, and the ion currents increase with power deposition as the plasma density increases. In general, the agreement between calculations and experiments is better at more negative probe voltages. These trends most likely result from two causes. First, the probe theory is more accurate for more negative probe voltages. Second, the location of the probe is within the presheath where the ion velocity distribution is anisotropic due to acceleration by the ambipolar electric field. The probe theory assumes an isotropic velocity distribution which, on the average, overestimates the probe area. These differences become less important at larger probe voltages. Consequently, we chose the probe collecting voltage to be −100 V for further comparisons and refer to this value as I_s.

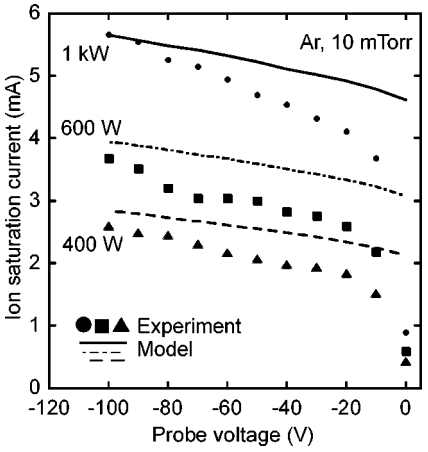

FIG. 7. Ion saturation currents vs probe collecting voltage in ICPs sustained in Ar; 40 sccm, $r_p = 0.05$ cm, $A_p = 0.11$ cm^2. The ion saturation currents depend on the probe voltage through the finite ratio of the sheath thickness to the probe radius.

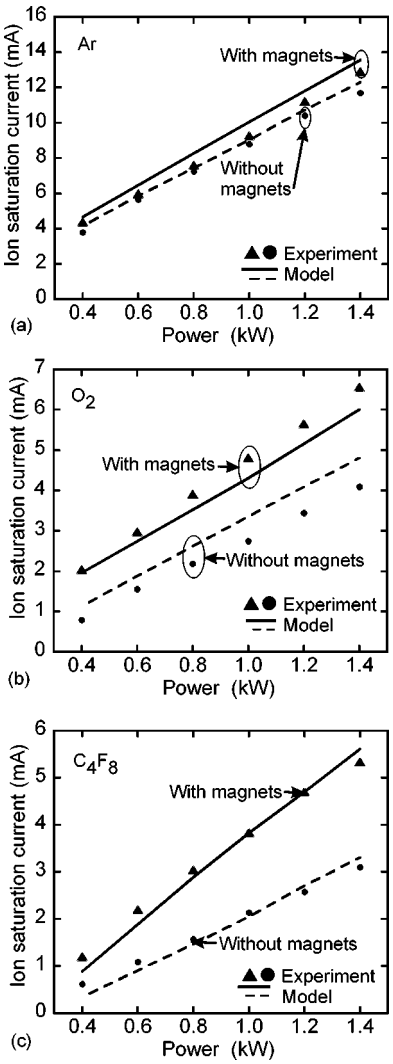

FIG. 8. Ion saturation currents as a function of power in ICPs sustained at 10 mTorr in (a) Ar, (b) O_2, and (c) c-C_4F_8; 40 sccm, $V_p = -100$ V, $r_p = 0.05$ cm, $A_p = 0.18$ cm^2. Linear increases of currents with power imply near linear increases of positive ion fluxes with power.

I_s as a function of power for ICPs with and without magnets sustained in 10 mTorr of Ar, O_2, and c-C_4F_8 are shown in Fig. 8. The agreement between experiments and calculations is favorable. Over the range of power investigated here, the ion saturation currents are nearly linearly proportional to power, indicating a nearly linear increase in ion densities. I_s

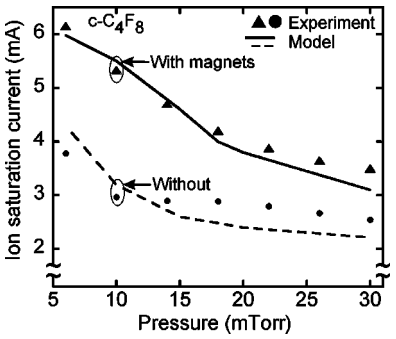

FIG. 9. Ion saturation currents as a function of pressure in ICPs sustained at 1.4 kW in c-C_4F_8; 40 sccm, $V_p=-100$ V, $r_p=0.05$ cm, $A_p=0.18$ cm^2. Currents are less effected by magnetic confinement at high pressure, where collision frequencies are commensurate with cyclotron frequencies.

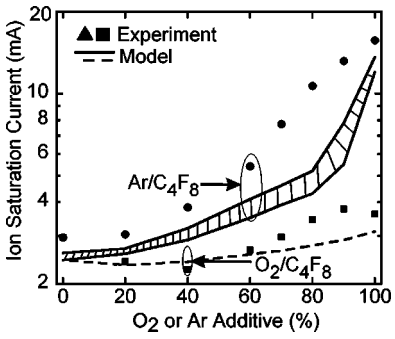

FIG. 10. Ion saturation currents in ICPs sustained at 1.4 kW in Ar/c-C_4F_8 and O_2/c-C_4F_8; 40 sccm, $V_p=-100$ V, $r_p=0.05$ cm, $A_p=0.18$ cm^2. Ion current increases faster with Ar addition than with O_2 addition as ionization processes are more efficient in Ar.

is proportional to the sum of the total contribution of the fluxes of positive ions which in turn depends on the mole fraction of ions having different thermal speeds. As the speeds of heavy ions are typically lower than those of light ions due to both mass and temperature, I_s is rather sensitive to the mole fraction of light ions.

I_s is generally larger with magnets as both the rate of loss of electrons and the loss rates of light positive ions on the wall decrease due to the reduction in cross field mobility. This latter effect is only important in the periphery of the plasma where the magnetic field is large. Larger proportional increases in I_s are seen in O_2 and c-C_4F_8 plasmas compared to Ar plasmas. The largest and the smallest ion saturation currents at any constant power are obtained in Ar and c-C_4F_8, respectively. Magnetic confinement at 1 kW produces 5%–10% increases in I_s in Ar, whereas these increases are 30%–70% in O_2, and 80%–90% in c-C_4F_8.

The increases in I_s with magnets are, in part, due to both a net reactor averaged increase in the ion densities and a redistribution of the ion densities due to power deposition extending deeper into the plasma. For example, the plasma density is more uniform (less peaked in the center of the plasma) with magnets reflecting a flattening of the plasma potential (see Fig. 15 of Paper I.[19]). These effects are less severe in Ar, thereby producing a less dramatic difference in I_s with and without magnets.

I_s in ICPs sustained in c-C_4F_8 with and without magnets as a function of pressure is shown in Fig. 9. Ion fluxes decrease with increasing pressure as the higher collisionality dissipates a constant power with a lower electron density. The effects of magnetic confinement are, on a fractional basis, nearly constant over this pressure range. The enhancement to ion fluxes is 1.4–1.6, somewhat higher at lower pressures. The Larmor radii of ions for magnetic field of 100 G are a few cm and commensurate with ion mean free paths. Confinement is in large part a result of a decreased ambipolar electric field as a consequence of the decreased electron mobility. To the degree that the electrons are more collisional at the higher pressures, the consequences of magnetic confinement can be expected to be smaller at higher pressure, though not significantly so for the range of pressures investigated here.

I_s in ICPs sustained in Ar/c-C_4F_8 and O_2/c-C_4F_8 at 1.4 kW and 20 mTorr are shown in Fig. 10. Two solid lines are used to show the range of uncertainty in the predictions because of the finite mesh size and placement of the probe. I_s significantly increases with addition of Ar due to two effects. First, the efficiency of electron-impact ionization for Ar is higher than that for c-C_4F_8 as a consequence of multi-step ionization from Ar($4s$). Ar($4s$) is quenched by nonionizing collisions upon addition of c-C_4F_8. Second, for a fixed power deposition, the higher collisionality of c-C_4F_8 requires a lower electron density to dissipate the same power. In contrast to Ar/c-C_4F_8 plasmas, I_s is less sensitive to the addition of O_2 to c-C_4F_8 plasmas as the ion currents obtained for the same conditions in c-C_4F_8 and O_2 plasmas are similar. These trends are due to the rate of power dissipation by electrons in the two gases being similar, though somewhat larger in c-C_4F_8, and the lack of significant multi-step ionization processes in O_2 which would be quenched by the addition of c-C_4F_8.

Although the predicted I_s for pure Ar and c-C_4F_8 separately agree well with experiments, the values for intermediate gas mixtures are less well captured. Some of this disparity may be attributed to uncertainty in the location of the probe as shown in Fig. 10. The majority of the disparity is likely due to a synergistic affect between Ar and c-C_4F_8 which has not been well captured in the present reaction mechanism. We parametrized rate coefficients for Penning and dissociative excitation transfer involving Ar*, and charge exchange reactions involving Ar^+ over the range of physical realizable values without obtaining significantly better agreement. A likely source of error is the disparities of surface reactions which feed back products to the plasma. These reactions may, for example, be catalyzed more efficiently by either Ar^+ or $C_nF_m^+$.

The plasma composition was also investigated based on calculated and measured ion fluxes sampled near the edge of the substrate at the location shown in Fig. 3(a). Relative fluxes of ion species for c-C_4F_8 plasmas with and without magnets are given in Table VI. Experiments are compared

TABLE VI. Fluxes of fluorocarbon ion species relative to that of CF^+ in c-C_4F_8 plasmas with and without magnets (6 mTorr, 600 W, 13.56 MHz).

Ion species	Experiment	Model[a] Version 1	Model[a] Version 2
Without magnets			
C^+	0.02	0.28	0.36
F^+	0.01	0.02	0.02
CF^+	1.00	1.00	1.00
CF_2^+	0.34	2.33	0.94
CF_3^+	0.61	0.11	0.71
$C_2F_3^+$	0.01	0.04	0.01
$C_2F_4^+$	0.38	0.32	0.13
$C_3F_5^+$	0.16	0.08	0.07
$C_4F_7^+$	0.01	0.02	0.005
With magnets			
C^+	7×10^{-4}	0.43	0.46
F^+	0.01	0.03	0.05
CF^+	1.00	1.00	1.00
CF_2^+	0.29	2.76	1.12
CF_3^+	0.17	0.07	0.68
$C_2F_3^+$	0.01	0.03	0.02
$C_2F_4^+$	0.03	0.21	0.11
$C_3F_5^+$	6×10^{-3}	0.04	0.03
$C_4F_7^+$	⋯	0.01	0.007

[a]The branching for electron impact dissociative excitation of C_2F_4 was CF_2+CF_2 for Version 1, and split equally between CF_2+CF_2 and $CF+CF_3$ for Version 2.

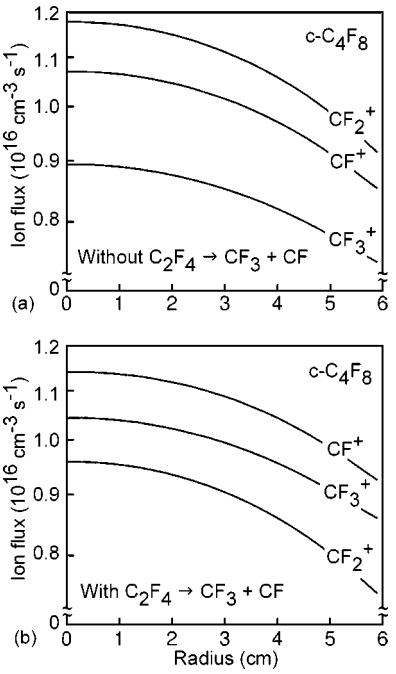

FIG. 11. Ion fluxes near the substrate (a) without and (b) with branching of C_2F_4 to $CF+CF_3$ at 10 mTorr, 600 W, 13.56 MHz, and 40 sccm. The branching for C_2F_4 dissociation has a first order effect on fluorocarbon ion fluxes.

with calculations obtained using two different branching ratios for C_2F_4 electron impact dissociation given by reactions in Eqs. (9) and (10). In both cases, the model predicts the same set of dominant ions as observed in experiments. Without magnets, experiments confirm the computationally observed abundance of $[C_2F_4^+]$ which supports the assumption for the initial electron impact dissociation channel branching of c-C_4F_8 being $C_2F_4+C_2F_4$. The computed $[CF_2^+]/[CF^+]$ and $[CF_3^+]/[CF^+]$ are in better agreement with experiments if the branching ratio for C_2F_4 dissociation is split equally between the reactions in Eqs. (9) and (10) implying that the branching ratios for the dissociation of C_2F_4 are critical to the reaction mechanism. With magnets the ratio of the heavy to light ion flux decreases due to a higher degree of dissociation, however we do not capture the increases observed experimentally. For example, the model predicts a 20%–30% decrease of $[C_2F_4^+]/[CF^+]$, whereas experiments show an order of magnitude decrease of $[C_2F_4^+]/[CF^+]$.

The branching ratios for C_2F_4 electron impact dissociation significantly affect the fluxes of the dominant fluorocarbon ions incident onto the substrate as shown in Fig. 11. Without the branching of C_2F_4 to CF_3 and CF, CF_2^+ has the largest flux to the substrate as a consequence of the resulting larger density of CF_2 and CF_2^+. The flux of CF_2^+ is lower than the fluxes of CF_3^+ and CF^+ if the branching to CF_3+CF has the same likelihood as to CF_2+CF_2. Consequently, the branching ratios for dissociative excitation of C_2F_4 are critical to the reaction mechanism.

Relative fluxes of ion species at the edge of the wafer for Ar/c-$C_4F_8=90/10$ plasmas with and without magnets are given in Table VII. The model overestimates the concentrations of heavy ions and underestimates the concentration of light ions which is likely due to the estimated rates of charge exchange reactions between Ar^+ and fluorocarbon radicals. With magnets the ratio of heavy ion flux to light ion flux decreases, similar to the trend observed in ICPs sustained in c-C_4F_8.

TABLE VII. Fluxes of fluorocarbon ion species relative to that of Ar^+ in Ar/c-$C_4F_8=90/10$ plasmas with and without magnets (6 mTorr, 600 W, 13.56 MHz).

Ion species	Experiment	Model
Without magnets		
Ar^+	1.000	1.000
C^+	0.096	0.003
F^+	0.007	0.001
CF^+	0.405	0.071
CF_2^+	0.516	0.094
CF_3^+	0.739	0.047
$C_2F_3^+$	0.007	0.003
$C_2F_4^+$	0.059	0.129
$C_3F_5^+$	0.020	0.089
$C_4F_7^+$	⋯	0.017
With magnets		
Ar^+	1.000	1.000
C^+	0.006	0.002
F^+	0.009	0.001
CF^+	0.240	0.043
CF_2^+	0.400	0.082
CF_3^+	0.325	0.052
$C_2F_3^+$	0.011	0.002
$C_2F_4^+$	0.025	0.116
$C_3F_5^+$	0.007	0.068
$C_4F_7^+$	0.002	0.019

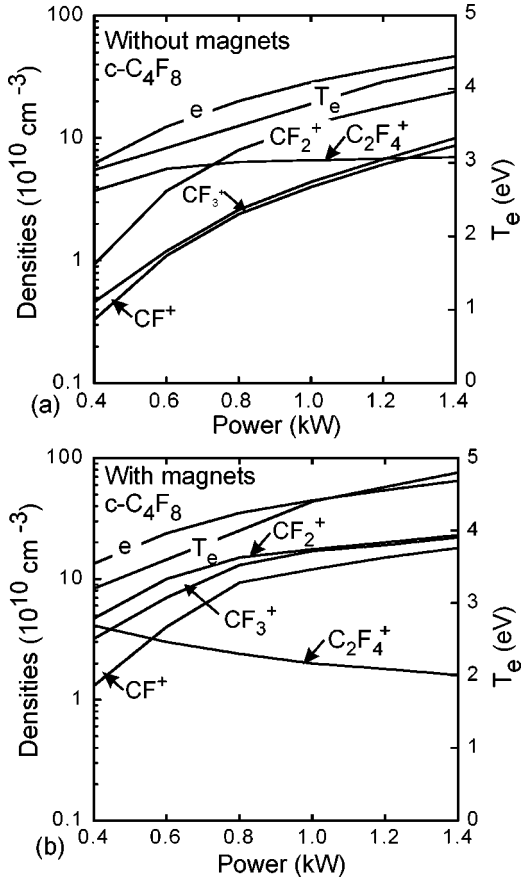

FIG. 12. Effect of power on the plasma properties in c-C_4F_8; 10 mTorr, 13.56 MHz, 40 sccm. (a) Without magnets and (b) with magnets. The ratio of heavy to light ion density decreases with increased power in ICP with magnets faster than without magnets.

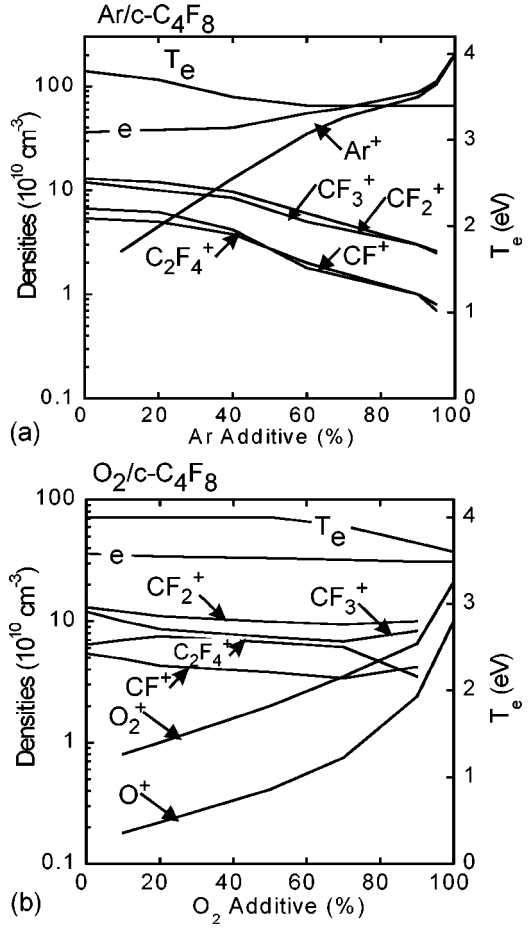

FIG. 13. Effect of Ar and O_2 addition on the plasma properties in (a) Ar/c-C_4F_8 and (b) O_2/c-C_4F_8; 20 mTorr, 1.4 kW, 13.56 MHz, 40 sccm. The densities of fluorocarbon species are more sensitive to Ar addition than to O_2 addition as the threshold of inelastic process for Ar (11.6 eV) is larger than the threshold of vibration processes for O_2 (less than eV).

The densities of the dominant light and heavy fluorocarbon ions and electron density as a function of power in c-C_4F_8 plasmas with and without magnets at the probe location are shown in Fig. 12. Without magnets the densities of CF^+, CF_2^+, CF_3^+, and [e] proportionally increase with power as a consequence of increased ionization and dissociation rates. $[C_2F_4^+]$ initially increases with power and then remains constant for powers above 800 W. These results imply that $[C_2F_4]$ and $[C_4F_8]$ decrease with power as $C_2F_4^+$ is dominantly produced by electron impact ionization of C_2F_4 and C_4F_8

$$e + C_4F_8 \rightarrow C_2F_4^+ + C_2F_4 + e + e, \tag{17}$$

$$e + C_2F_4 \rightarrow C_2F_4^+ + e + e. \tag{18}$$

With magnets $[CF^+]$ increases more rapidly with power than $[CF_2^+]$ and $[CF_3^+]$ due to the greater degree of fragmentation of the feedstock. $[C_2F_4^+]$ decreases as power increases confirming that $[C_4F_8]$ and $[C_2F_4]$ effectively dissociate into smaller fluorocarbon radicals for ICPs with magnets. T_e rapidly increases with power in both cases. This is attributed to the CF_x species which are formed in c-C_4F_8 plasmas as a result of dissociation and whose efficiencies for ionization are typically smaller than that of c-C_4F_8. T_e increases more rapidly for ICPs with magnets as dissociation in such a system is more efficient.

Recall that probe and mass spectroscopy usually measure fluxes of ions (or radicals) which must be corrected for collection speed to obtain densities. Small fluxes of heavy fluorocarbon ions do not necessarily imply that their densities are equally small in the gas phase. Assuming equal temperatures (lighter ions usually have larger temperatures) fluxes generally scale inversely with $M^{-1/2}$ and so the density of heavy ions (e.g., $C_2F_4^+$ vs CF^+) relative to light ions can be a factor of 2 larger than indicated by their fluxes.

The density of the dominant fluorocarbon ions, $[Ar^+]$, and [e] as a function of Ar and O_2 fractions in Ar/c-C_4F_8 and O_2/c-C_4F_8 plasmas is shown in Fig. 13. Initially, the electron density remains almost constant and the densities of fluorocarbon ions only slightly decrease as the fraction of Ar increases implying that dissociation and ionization rates of fluorocarbons are not significantly affected by small changes in Ar fraction. The proportion of power that is channeled into Ar is small. Electrons preferentially expend their energies on the dissociation and ionization of fluorocarbons as

the thresholds of these processes are a few eV lower than the Ar ionization threshold. $[Ar^+]$ is about the same as the densities of the dominant fluorocarbon ions when the Ar fraction reaches 40%. At larger Ar fractions, the densities of fluorocarbon ions decrease and [e] and $[Ar^+]$ rapidly increase as the fraction of power dissipated in the electron impact ionization collisions with Ar becomes significant. T_e decreases from 4.8 to 4.3 eV with increased Ar fraction as ionization processes are more efficient in Ar plasma than in highly dissociated c-C_4F_8 plasma.

The electron density and densities of fluorocarbon ions weakly depend on the fraction of O_2 in O_2/c-C_4F_8 plasmas as electrons preferably ionize and dissociate fluorocarbon species due to their ionization and dissociation thresholds being lower than those of O_2. Consequently, $[O_2^+]$ and $[O^+]$ exceed the density of fluorocarbon ions only for O_2 fractions >0.9. T_e decreases with increased O_2 fraction as ionization processes are more efficient in O_2 compared to c-C_4F_8.

V. CONCLUDING REMARKS

A reaction mechanism involving electron impact and heavy particle reactions for low-pressure and low-temperature plasmas sustained in mixtures initially consisting of Ar/c-$C_4F_8/O_2/CO$ was developed. It was found that charge exchange reactions of Ar^+ and CO^+ with fluorocarbon species significantly affect the ratio of light to heavy fluorocarbon ions in Ar/c-$C_4F_8/O_2/CO$ mixture. Predicted plasma properties were validated by comparing to experiments in magnetically enhanced low-pressure ICPs. Computed results well represented the measured ion saturation currents in ICPs sustained in Ar, O_2, Ar/c-C_4F_8 and O_2/c-C_4F_8 and reproduced major trends obtained from ion spectra measurements for ICPs sustained in c-C_4F_8 and Ar/c-C_4F_8. We found that ion currents increase with the addition of Ar to c-C_4F_8 and weakly depend on the addition of O_2 to c-C_4F_8. Also, the ratio of light ion to heavy ion densities increases with power, especially for ICP with static magnets.

ACKNOWLEDGMENTS

This work was supported by the International SEMATCH and the Semiconductor Research Corp. The works of X.L. and G.S.O. were additionally supported by the Department of Energy (Contract No. DE-FG0200ER54608). A.V.V. and M.J.K. were also supported by the National Science Foundation (CTS99-74962 and CTS03-15353) and CFD Research Corp. The authors thank Dr. Vivek Bakshi for helpful discussions.

[1]K. Miyata, M. Hori, and T. Goto, J. Vac. Sci. Technol. A **15**, 568 (1997).
[2]J.-P. Booth, Plasma Sources Sci. Technol. **8**, 249 (1999).
[3]M. Sekine, Appl. Surf. Sci. **192**, 270 (2002).
[4]X. Li, L. Ling, X. Hua, M. Fukasawa, and G. S. Oehrlein, J. Vac. Sci. Technol. A **21**, 284 (2003).
[5]K. Sasaki, Y. Kawai, C. Suzuki, and K. Kadota, J. Appl. Phys. **83**, 7482 (1998).
[6]M. Matsui, T. Tatsumi, and M. Sekine, J. Vac. Sci. Technol. A **19**, 2089 (2001).
[7]G. S. Oehrlein, M. F. Doemling, B. E. E. Kastenmeier, P. J. Matsuo, N. R. Rueger, M. Schaepkens, and T. E. F. M. Standaert, IBM J. Res. Dev. **43**, 181 (1999).
[8]M. Matsui, T. Tatsumi, and M. Sekine, J. Vac. Sci. Technol. A **19**, 1282 (2001).
[9]L. G. Christophorou, J. K. Olthoff, and M. V. V. S. Rao, J. Phys. Chem. Ref. Data **25**, 1341 (1996).
[10]L. G. Christophorou and J. K. Olthoff, J. Phys. Chem. Ref. Data **27**, 889 (1998).
[11]L. G. Christophorou and J. K. Olthoff, J. Phys. Chem. Ref. Data **27**, 1 (1998).
[12]L. G. Christophorou and J. K. Olthoff, J. Phys. Chem. Ref. Data **30**, 449 (2001).
[13]P. Ho, J. E. Johannes, R. J. Buss, and E. Meeks, J. Vac. Sci. Technol. A **19**, 2344 (2001).
[14]G. I. Font, W. L. Morgan, and G. Mennenga, J. Appl. Phys. **91**, 3530 (2002).
[15]K. Yoshida, S. Goto, H. Tagashira, C. Winstead, B. V. McKoy, and W. L. Morgan, J. Appl. Phys. **91**, 2637 (2002).
[16]S. Rauf and P. L. G. Ventzek, J. Vac. Sci. Technol. A **20**, 14 (2002).
[17]H. Kazumi, R. Hamasaki, and K. Tago, Plasma Sources Sci. Technol. **5**, 200 (1996).
[18]G. A. Hebner, J. Appl. Phys. **90**, 4938 (2001).
[19]X. Li, L. Ling, X. Hua, G. S. Oehrlein, A. V. Vasenkov, and M. J. Kushner (unpublished).
[20]A. V. Vasenkov and M. J. Kushner, Phys. Rev. E **66**, 066411 (2002).
[21]L. Schott, in *Plasma Diagnostics* (Wiley, New York, 1968).
[22]M. A. Lieberman and A. J. Lichtenberg, *Principles of Plasma Discharges and Materials Processing* (Wiley, New York, 1994).
[23]W. W. Stoffels, E. Stoffels, and K. Tachibana, J. Vac. Sci. Technol. A **16**, 87 (1998).
[24]S. Sasaki, Y. Hirose, I. Ishikawa, K. Nagaseki, Y. Saito, and S. Suganomata, Jpn. J. Appl. Phys., Part 1 **36**, 5296 (1997).
[25]K. Teii, M. Hori, M. Ito, T. Goto, and N. Ishii, J. Vac. Sci. Technol. A **18**, 1 (2000).
[26]W. Schwarzenbach, G. Cunge, and J. P. Booth, J. Appl. Phys. **85**, 7562 (1999).
[27]A. N. Goyette, Y. Wang, M. Misakian, and J. K. Olthoff, J. Vac. Sci. Technol. A **18**, 2785 (2000).
[28]E. R. Fuoco and L. Hanley, J. Appl. Phys. **92**, 37 (2002).
[29]K. Tachibana, Phys. Rev. A **34**, 1007 (1986).
[30]D. Rapp and P. Englander-Golden, J. Chem. Phys. **43**, 1464 (1965).
[31]R. H. McFarland and J. D. Kinney, Phys. Rev. **137**, 1058 (1965).
[32]I. P. Zapesochnyi, Y. N. Semenyuk, A. I. Dashchenko, A. E. Imre, and A. I. Zapesochny, JETP Lett. **39**, 141 (1984).
[33]L. Vriens, Phys. Lett. **8**, 260 (1964).
[34]A. V. Phelps, JILA Information Center Report No. 28, University of Colorado, 1985.
[35]E. Krishnakumar and S. K. Srivastava, Int. J. Mass Spectrom. Ion Processes **113**, 1 (1992).
[36]E. Brook, M. F. A. Harrison, and A. C. H. Smith, J. Phys. B **11**, 3115 (1978).
[37]W. Liu and G. A. Victor, Astrophys. J. **435**, 909 (1994).
[38]W. L. Morgan (private communication), Kinema Software, http://www.kinema.com
[39]M. Hayashi and T. Nimura, J. Appl. Phys. **54**, 4879 (1983).
[40]V. Tarnovsky and K. Becker, J. Chem. Phys. **98**, 7868 (1993).
[41]V. Tarnovsky, P. Kurunczi, D. Rogozhnikov, and K. Becker, Int. J. Mass Spectrom. Ion Processes **128**, 181 (1993).
[42]R. A. Bonham, Jpn. J. Appl. Phys., Part 1 **33**, 4157 (1994).
[43]M. Gryzinski, Phys. Rev. **138**, 336 (1965).
[44]V. Tarnovsky, H. Deutsch, and K. Becker, J. Phys. B **32**, L573 (1999).
[45]M. Hayashi and A. Niwa, in *Gaseous Dielectrics V*, edited by L. G. Christophorou and D. W. Bouldin (Pergamon, New York, 1987), pp. 27–33.
[46]R. A. Morris, A. A. Viggiano, S. T. Arnold, and J. F. Paulson, Int. J. Mass Spectrom. Ion Processes **149/150**, 287 (1995).
[47]C. Q. Jiao, A. Garscadden, and P. D. Haaland, Chem. Phys. Lett. **297**, 121 (1998).
[48]A. Jain and D. W. Norcross, Phys. Rev. A **45**, 1644 (1992).
[49]M. Hayashi, Nagoya Institute of Technology Report, No. IPPJ-AM-19, 1991.
[50]C. Winstead and V. McKoy, J. Chem. Phys. **114**, 7407 (2001).

[51]I. Sauers, L. G. Christophorou, and J. G. Carter, J. Chem. Phys. **71**, 3016 (1979).
[52]R. L. Woodin, M. S. Foster, and J. L. Beauchamp, J. Chem. Phys. **72**, 4223 (1980).
[53]P. W. Harland and J. L. Franklin, J. Chem. Phys. **61**, 1621 (1974).
[54]J. E. Sanabia, G. D. Cooper, J. A. Tossell, and J. H. Moore, J. Chem. Phys. **108**, 389 (1998).
[55]H. S. Porter, C. H. Jackman, and A. E. S. Green, J. Chem. Phys. **65**, 154 (1976).
[56]H. Toyoda, M. Iio, and H. Sugai, Jpn. J. Appl. Phys., Part 1 **36**, 3730 (1997).
[57]S. H. Bauer and S. Javanovic, Int. J. Chem. Kinet. **30**, 171 (1998).
[58]A. Yokoyama, K. Yokoyama, and G. Fujisawa, Chem. Phys. Lett. **237**, 106 (1995).
[59]C. Winstead and V. McKoy, J. Chem. Phys. **116**, 1380 (2002).
[60]J. T. Moseley, R. E. Olson, and J. R. Peterson, Case Stud. At. Phys. **5**, 1 (1975).
[61]A. P. Hickman, J. Chem. Phys. **70**, 4872 (1979).
[62]Y. Itikawa, A. Ichimura, K. Onda, K. Sakimoto, K. Takayanagi, Y. Hatano, M. Hayashi, H. Nishimura, and S. Tsurubuchi, J. Phys. Chem. Ref. Data **18**, 23 (1989).
[63]E. Meeks, R. S. Larson, P. Ho, C. Apblett, S. M. Han, E. Edelberg, and E. S. Aydil, J. Vac. Sci. Technol. A **16**, 544 (1998).
[64]NIST Chemical Kinetics Database.
[65]E. Meeks, J. Electrochem. Soc. **144**, 357 (1998).
[66]L. G. Piper, J. E. Velazco, and D. W. Setser, J. Chem. Phys. **59**, 3323 (1973).
[67]D. L. King, L. G. Piper, and D. W. Setser, J. Chem. Soc., Faraday Trans. A **73**, 177 (1977).
[68]J. E. Velazco, J. H. Kolts, and D. W. Setser, J. Chem. Phys. **65**, 3468 (1976).
[69]A. N. Klucharev and V. Vujnovic, Phys. Rep. **185**, 55 (1990).
[70]H. W. Ellis, R. Y. Pai, E. W. McDaniel, E. A. Mason, and L. A. Viehland, At. Data Nucl. Data Tables **17**, 177 (1976).
[71]B. F. Gordiets, C. M. Ferreira, V. L. Guerra, J. M. A. H. Loureiro, J. Nahorny, D. Pagnon, M. Touzeau, and M. Vialle, IEEE Trans. Plasma Sci. **23**, 750 (1995).
[72]R. Atkinson, D. L. Baulch, R. A. Cox, R. F. Hampson, Jr., J. A. Kerr, M. J. Rossi, and J. Troe, J. Phys. Chem. Ref. Data **26**, 521 (1997).
[73]J. T. Herron and D. S. Green, Plasma Chem. Plasma Process. **21**, 459 (2001).
[74]G. Dorthe, P. Caubet, T. Vias, B. Barrere, and J. Marchais, J. Phys. Chem. **95**, 5109 (1991).
[75]R. R. Baldwin, D. Jackson, A. Melvin, and B. N. Rossitero, Int. J. Chem. Kinet. **4**, 277 (1972).
[76]D. R. Burgess, M. R. Zachariah, W. Tsang, and P. R. Westmoreland, Prog. Energy Combust. Sci. **21**, 453 (1996).
[77]K. Yamasaki, A. Tanaka, A. Watanabe, K. Yokoyama, and I. Tokue, J. Phys. Chem. **99**, 15086 (1995).
[78]NIST Standard Reference Database 17, Institute of Standards and Technology, 1998.
[79]J. T. Herron, J. Phys. Chem. Ref. Data **17**, 967 (1988).
[80]R. J. Cvetanovic, J. Phys. Chem. Ref. Data **16**, 261 (1987).
[81]K. R. Ryam and I. C. Plumb, Plasma Chem. Plasma Process. **4**, 271 (1984).
[82]N. Haider and D. Husain, Int. J. Chem. Kinet. **25**, 423 (1993).
[83]I. C. Plumb and K. R. Ryan, Plasma Chem. Plasma Process. **6**, 205 (1986).
[84]P. K. Chowdhury, K. V. S. R. Rao, and J. P. Mittal, J. Phys. Chem. **92**, 102 (1988).
[85]K. Okada, O. Kajimoto, and T. Fueno, Chem. Soc. Jpn. Bull. **51**, 443 (1978).
[86]I. C. Plumb and K. R. Ryan, Plasma Chem. Plasma Process. **9**, 409 (1989).
[87]C. Tsai, S. M. Belanger, J. T. Kim, J. R. Lord, and D. L. McFadden, J. Phys. Chem. **93**, 1916 (1989).
[88]N. I. Butkovskaya, M. N. Larichev, I. O. Leipunskii, I. I. Morozov, and V. L. Talroze, Kinet. Katal. **21**, 263 (1980).
[89]K. R. Ryan and I. C. Plumb, Plasma Chem. Plasma Process. **6**, 231 (1986).
[90]E. L. Keating and R. A. Matula, J. Chem. Phys. **66**, 1237 (1977).
[91]V. L. Orkin and A. M. Chaikin, Kinet. Katal. **23**, 438 (1982).
[92]D. C. Parent, R. Derai, G. Mauclaire, M. Heninger, R. Marx, M. E. Rincon, A. O'Keefe, and M. T. Bowers, Chem. Phys. Lett. **117**, 127 (1985).
[93]P. Gaucherel, Int. J. Mol. Spectrosc. **25**, 211 (1977).
[94]E. R. Fisher, M. E. Weber, and P. B. Armentrout, J. Chem. Phys. **92**, 2296 (1990).
[95]D. Smith and L. Kevan, J. Chem. Phys. **55**, 2290 (1971).
[96]D. P. Almeida, A. C. Fontes, and C. F. L. Godinho, J. Phys. B **28**, 3335 (1995).
[97]R. A. Morris, A. A. Viggiano, and J. F. Paulson, J. Phys. Chem. **97**, 6208 (1993).
[98]R. A. Morris, A. A. Viggiano, J. M. Van Doren, and J. F. Paulson, J. Phys. Chem. **96**, 2597 (1992).
[99]G. K. Jarvis, C. A. Mayhew, and R. P. Tuckett, J. Phys. Chem. **100**, 17166 (1996).
[100]G. K. Vinogradov, P. I. Verzorov, L. S. Polak, and K. I. Slovetsky, Vacuum **32**, 592 (1982).
[101]Y. Ikezoe, S. Matsuoka, M. Takebe, and A. Viggiano, *Gas-Phase Ion-Molecular Reaction Rate Constants Through 1986* (Maruzen, Tokyo, 1987).
[102]C. A. Mayhew and D. Smith, Int. J. Mass Spectrom. Ion Processes **100**, 737 (1990).
[103]E. R. Fisher and P. B. Armentrout, J. Phys. Chem. **95**, 6118 (1991).
[104]R. E. Olson, J. R. Peterson, and J. Moseley, J. Chem. Phys. **53**, 3391 (1970).
[105]M. A. Biondi, in *Principles of Laser Plasmas*, edited by G. Bekefi (Wiley, New York, 1976).